Chapter 5

Buckling and Postbuckling responses of Hybrid Composite Plates under In-plane Shear Load

5.1. Introduction

This chapter deals with the numerical study of postbuckling response and strength of functionally graded hybrid composite plates as well as effect of different boundary conditions under the application of in-plane shear loads. With an ever-increasing need for functional materials, there has been a major research effort to develop advanced composite materials such as functionally graded materials (FGM) knowing the fact that single phase materials have a finite scope of implementation. In this chapter, numerical study of buckling and postbuckling responses of functionally graded composite plates with and without cutouts are investigated. The orientation of the fiber aligned in ($0^o/90^o$), ($+45^o/-45^o$), and ($+45^o/-45^o/0^o/90^o$) are considered for all the plates simulated. In addition, effect of different boundary conditions on postbuckling response are considered.

In the current chapter, flexural and in-plane boundary conditions are considered to study their effects on buckling and postbuckling responses of functionally graded hybrid plate with and without cutouts subjected to positive and negative in-plane shear loads. The quasi-isotropic $(\pm 45/0/90)_{2s}$ layup sequence is considered in the plate for the numerical investigation with various shaped cutouts. The flexural boundary conditions include all four edges simply supported, two edges simply supported, and two edges clamped, and all four edges clamped while the in-plane boundary conditions consist of variation of in-plane boundary restraints for all edges simply supported. The analysis is based on finite element method-based software ABAQUS.

It may be noted that, a detailed experimental study has also been performed and results have been shown in the published document for patent application as per list of publication.

5.2. Numerical approach

Finite element analysis-based software (ABAQUS) is used for simulating the functionally graded hybrid (FH) plates under positive and negative in-plane shear loads. Linear and non-linear

buckling and postbuckling numerical analysis of the square symmetric plate with the influence of imperfections are presented. In the first step, Eigen value linear buckling analysis approach has been used to determine critical buckling load. Prior to buckling, a very little deformation occurs depending on the magnitude of imperfection. After the linear buckling analysis, non-linear buckling analysis has been performed using static-riks method in which load is incremented using a load proportionality factor (LPF) and the structure is configured using an arc length method which allows the procedure to follow the direction of load. This implies that a static-riks step cannot end after a certain pre-prescribed load. Therefore, the procedure ends after reaching a maximum LPF. The behavior of the material is elasto-plastic during nonlinear analysis. To obtain more realistic information of postbuckling response, imperfections are considered. Type of imperfections considered in this study is geometric imperfections. Imperfections highly influence the stability behavior of the plates under the applied load. Plate is modelled with four-noded linear shell elements (S4R) with reduced integration in modeling the structure in the current analysis. Finer mesh is used in the current study to produce reasonable accuracy in plate with and without cutouts. Meshing was done to the plate with an approximate element size of 0.004. Thereafter, Tsai-Hill failure criterion has been incorporated in the step module of non-linear buckling analysis for determining first ply failure load which corresponds to first failure in a ply in the plate after the loading is applied. In ABAQUS numerical study, ultimate failure load is occured at a point where the plate becomes unstable. Geometrically nonlinear problems sometimes involve buckling or collapse behavior. Abaqus offers an automated version of the stabilization approach for the static analysis procedures. Unstable phase of the response can be found by using the modified riks method.

The Riks method can be used to solve postbuckling problems both with stable and unstable behaviours. To analyze a postbuckling problem, it must be turned into a problem with continuous response instead of bifurcation. This effect can be accomplished by introducing an initial imperfection into a “perfect” geometry so that there is some response in the buckling mode before the critical load is reached. This method is used for cases where the loading is proportional i.e., where the load magnitudes are governed by a single scalar parameter (load proportionality factor). This method can provide solutions even in cases of complex and unstable response. In case of problems with material non-linearity, geometric non-linearity prior to buckling or unstable postbuckling response, load-deflection riks analysis must be performed to investigate the problem

further. To measure the progress of the solution, arc length quantity is used along the static equilibrium path in load-displacement space. This arc length approach provides solution regardless stable or unstable response. The plate reaches the ultimate load carrying capacity at a specified degree of freedom where it reaches a maximum value of load proportionality factor or a maximum dispacement value. In the current research maximum load magnitude has been considered, further the plate becomes unstable and the drop in load begins.

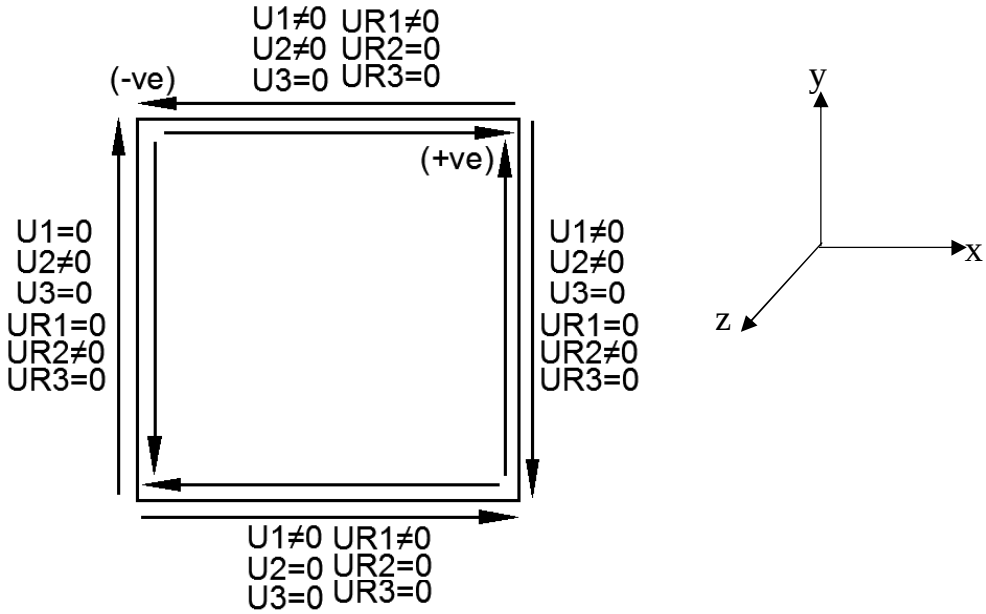

(a) FBC-1

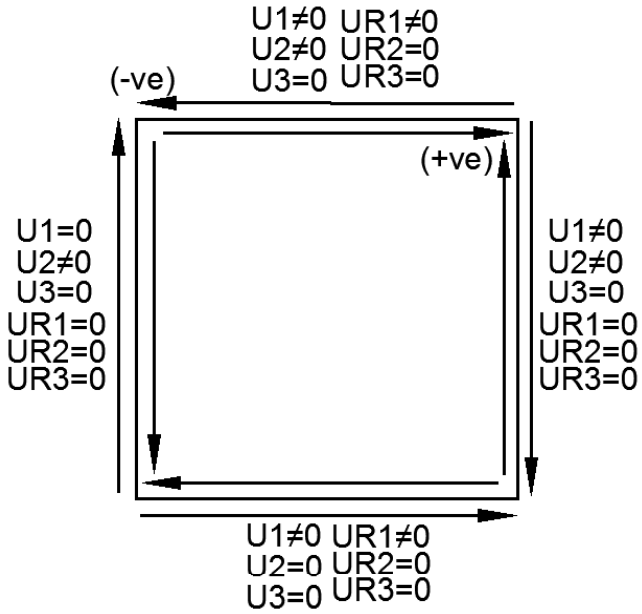

(b) FBC-2

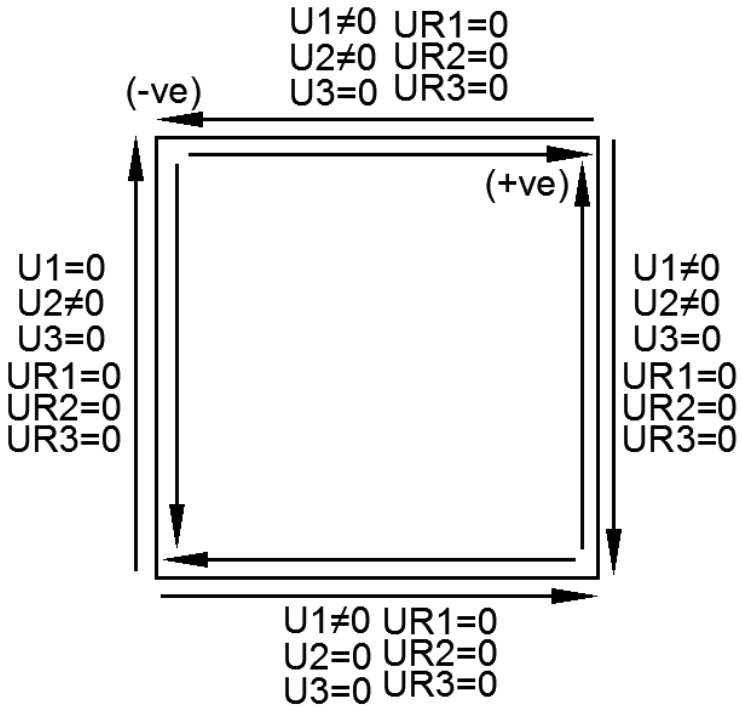

(c) FBC-3

Fig. 5.1. Details of flexural boundary conditions: (a) FBC1: Simply supported on all the edges; (b) FBC2: Simply supported on two edges and clamped on other two edges; (c) FBC3: Clamped on all the edges

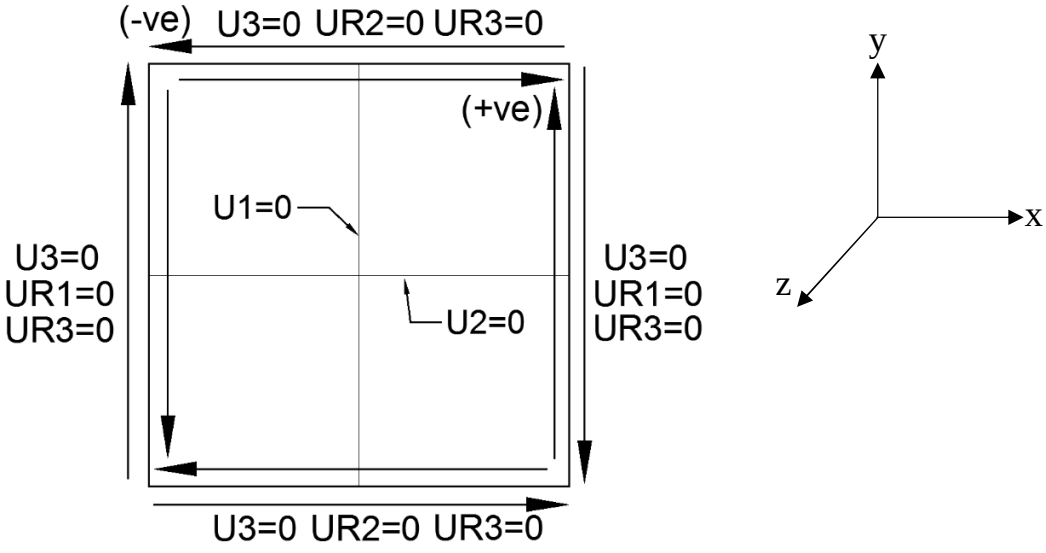

(a) PBC1

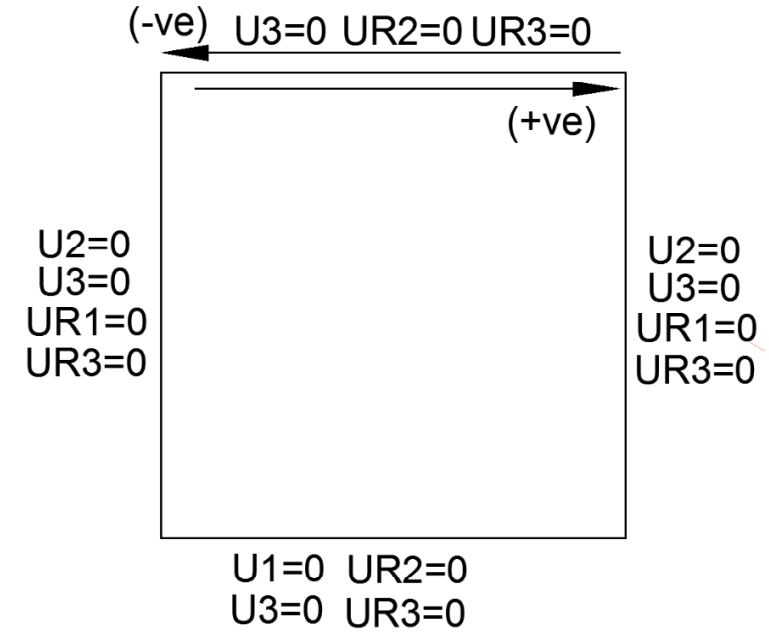

(b) PBC2

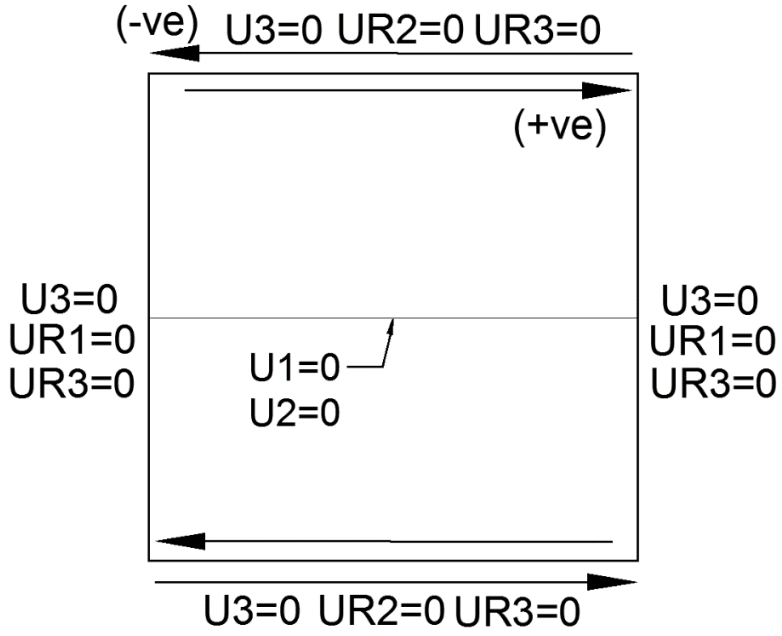

(c) PBC3

Fig. 5.2. Details of in-plane simply supported boundary conditions with in-plane boundary restraints: (a) PBC1; (b) PBC2 (c) PBC3

The flexural and in-plane boundary conditions used in this study are shown in Figs. 5.1 and 5.2, respectively. The flexural boundary conditions include all edges simply supported (x=0, x=b, y=0, y=b) (FBC1), simply supported on two edges (y=0, y=b) and clamped on other two (x=0, x=b) (FBC2), and all edges clamped (x=0, x=b, y=0, y=b) (FBC3) as shown in Figs. 5.1(a), 5.1(b) and

5.1(c), respectively. In case of in-plane boundary conditions all the edges are simply supported while keeping different in-plane boundary restraints as designated by PBC1, PBC2 and PBC3 shown in Figs. 5.2(a), 5.2(b), and 5.2(c), respectively.

5.3. Verification of numerical model

To check the accuracy of the numerical analysis performed in the present study, validation has been done with the FEM formulation results published by Kumar and Singh, 2010. Authors (Kumar and Singh, 2010) investigated the buckling and postbuckling responses of T300/5208 (pre-peg) graphite-epoxy material with and without cutouts under in-plane shear loads. The results shown in their study (Kumar and Singh, 2010) are based on a self-developed finite element program. The material properties, cutout specifications, boundary conditions and mesh sizes are taken into consideration and analyzed using the numerical method (ABAQUS) incorporated in the present chapter.

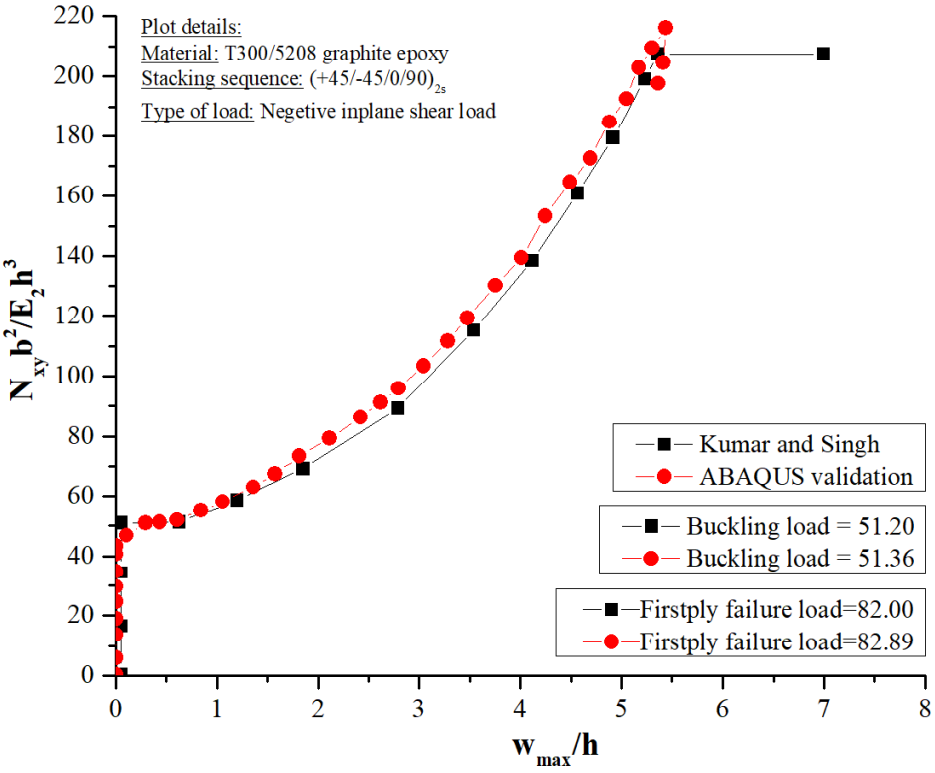

Fig. 5.3. Data validation of Kumar and Singh, 2010 with the numerical method (ABAQUS) used in this study

The stacking sequence of the plate used is $(+45/-45/0/90)_{2s}$. Validation of results have been done with ABAQUS and the non-dimensional buckling load ($N_{xy}b^2/E_2h^3$) vs. displacement (w_{max}/h) plot

is shown in Fig. 5.3. The non-dimensional buckling load obtained from the numerical analysis is 51.36 which is 0.3% higher. The first ply failure load obtained is 82.89 which is 1.07% higher. Hence it is clear that the validated results obtained using ABAQUS are in good agreement with the published results (Kumar and Singh, 2010).

5.4. Results and discussion

The numerical results of the FH plates simply supported on all the four edges with and without cutouts having fiber aligned in different directions are discussed below.

5.4.1. Critical buckling load

Plain carbon fiber reinforced polymer (CFRP), glass fiber reinforced polymer (GFRP), and functionally graded hybrid (FH) plates are simulated initially using Eigen value buckling analysis. The critical buckling loads (CBL) with fiber aligned in (0/90), (+45/-45), and (+45/-45/0/90) directions are determined and are presented in Table 5.1. The load vs. displacement plots of plates without cutouts is shown in Fig. 5.4. Functionally graded hybrid composite plate is a combination of carbon and glass fibers. Though, FH plate consists of 50% carbon fibers, the response of FH plate is closer to that of plain CFRP. Similar trend is observed in all the FH plates with various stacking sequences as shown in Fig. 5.4(a)–5.4(f) which represents the efficiency of functionally graded hybrid composite plates. As shown in Fig. 5.4(a)–5.4(f), the functionally graded hybrid plates of different fiber orientations have their strength and stiffness very close to that of CFRP plates with corresponding fiber orientations. The reason behind this observation is the surface of the FH plates is made of carbon fiber.

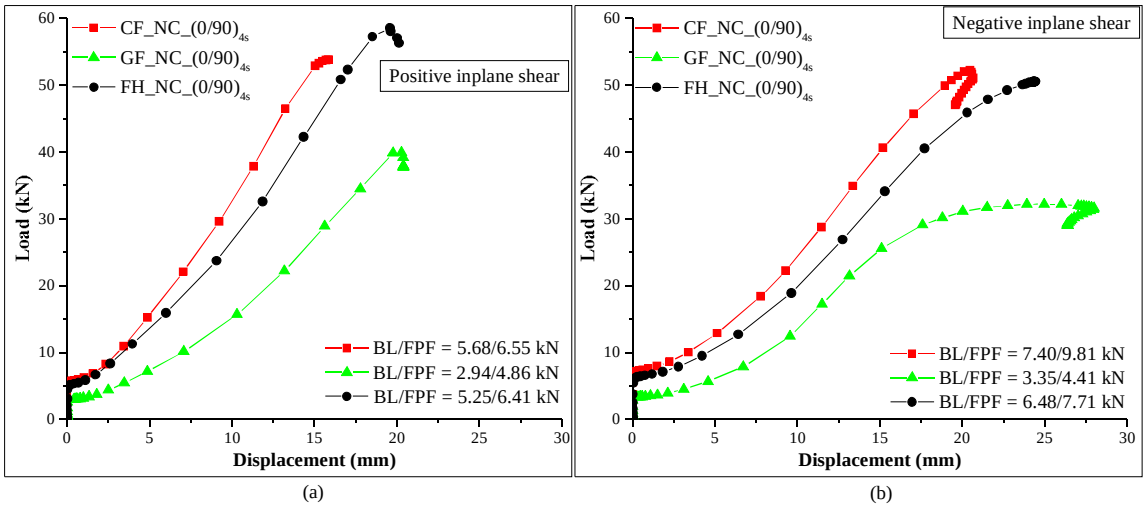

(a) (b)

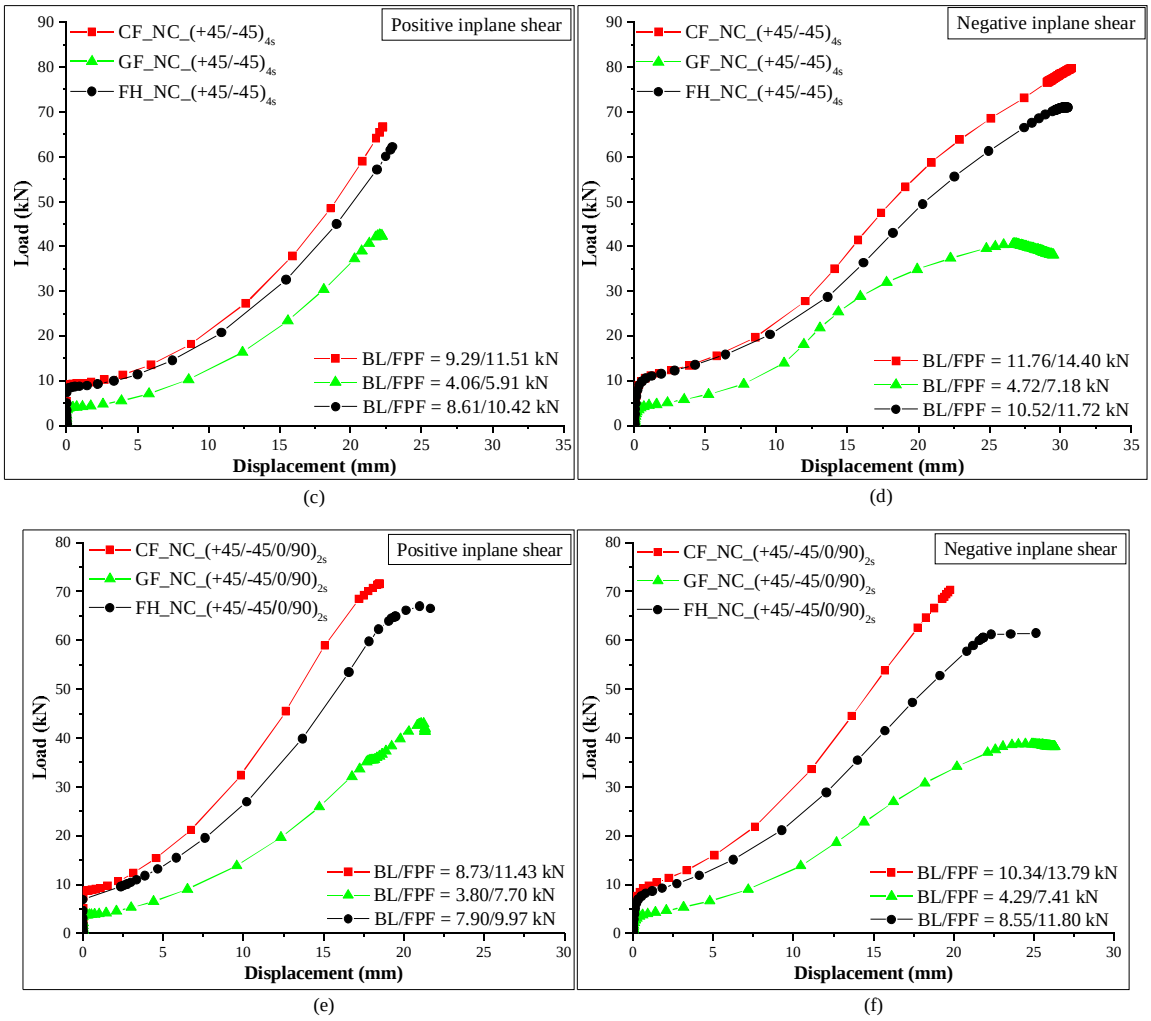

Fig. 5.4. Load vs. displacement plots of functionally graded hybrid plates with respect to carbon and glass fiber reinforced polymer plates with fiber aligned in: (a) (0/90) direction under positive in-plane shear load (b) (0/90) direction under negative in-plane shear load (c) (+45/-45) direction under positive in-plane shear load (d) (+45/-45) direction under negative in-plane shear load (e) (+45/-45/0/90) direction under positive in-plane shear load (f) (+45/-45/0/90) direction under negative in-plane shear load

The strength of the hybrid plate depends on the material present in the surface region. However, this represents the structural efficiency of FH plates with economy as amount of carbon fiber is reduced significantly. In Fig. 5.4(a) and 5.4(b), the composite plates aligned in (0/90) fiber direction are observed to have peak load higher than CFRP plate under positive in-plane shear and it is almost near to the peak load of CFRP in case of negative in-plate shear, respectively.

Table 5.1. Buckling loads of functionally graded hybrid plates with fiber aligned in $(0/90)_{4s}$, $(+45/-45)_{4s}$, and $(+45/-45/0/90)_{2s}$ directions with and without cutouts

Specimen ID / Orientation	Buckling load (kN) $(0/90)_{4s}$	$(+45/-45)_{4s}$	$(+45/-45/0/90)_{2s}$
FH_NC	8.34	4.98	7.55
FH_C1	8.17	4.73	7.31
FH_C2	7.51	4.07	6.57
FH_C3	6.14	3.36	5.52
FH_D1	8.24	4.86	7.43
FH_D2	7.90	4.50	7.08
FH_D3	7.27	3.95	6.49
FH_EH1	8.22	4.71	7.30
FH_EH2	7.73	4.02	6.54
FH_EH3	6.75	3.31	5.49
FH_EV1	8.07	4.71	7.28
FH_EV2	7.13	4.02	6.47
FH_EV3	5.37	3.31	5.29
FH_S1	8.16	4.69	7.26
FH_S2	7.44	3.99	6.39
FH_S3	5.94	3.40	5.37

The buckling mode shapes such as Mode I, II and III obtained post linear analysis under positive and negative in-plane shear loads are depicted in Fig. 5.5(a) and Fig. 5.5(b), respectively. Mode-I is the most critical and the values corresponding to this mode are taken. The maximum critical buckling load is obtained in case of functionally graded hybrid plate without cutout which is expected since most of the plates fails in the vicinity of cutouts. The load vs. displacement plot of FH plates without cutouts under positive and negative in-plane shear load is shown in Fig. 5.6(a) and (b) for laminates with different fiber orientations, respectively. The buckling and first ply failure loads are depicted in the figure itself. It is observed that the plate with fiber aligned in $(+45/-45)_{4s}$ direction has higher critical buckling and first ply failure load with respect to the plates with other stacking sequences as shown in Fig. 5.6(a). Similar trend is observed in FH plates subjected to negative in-plane shear load. The ultimate failure load is observed to be low in case of fiber aligned in (0/90) direction in both loading conditions. The failure buckling mode shapes of FH plates with and without cutouts under positive in-plane shear are presented in Fig. 5.7 (a) – 5.8 (p) and the FH plates under negative in-plane shear are presented in Fig. 5.8(a) –5.8 (p). Fig. 5.9 depicts the critical buckling load values of FH plates with small-sized (small sized) cutouts with

fiber aligned in all the three stacking sequences. As expected, it is observed that the plate without cutouts have higher buckling loads than the plates with cutouts. Plates analyzed under negative in-plane shear perform better in comparison with the plates under positive in-plane shear as shown in Figs. 5.6 and 5.7. It is also observed that the plate with fiber aligned in (+45/-45) direction has the highest buckling load in all the plates analyzed. Further, amongst the FH plates with cutouts, maximum critical buckling load is observed in plate with diamond shape having small-sized cutout. Plate FH_D1_$(+45/-45)_{4s}$ has 8.13% lesser buckling load with respect to the plate FH_NC_$(+45/-45)_{4s}$ under positive in-plane shear while it is 7.88% lesser in case of negative in-plane shear. In case of FH plates with medium-sized cutouts (Fig. 5.10), similar trend is observed, however the difference is higher. The FH_D2_$(+45/-45)_{4s}$ plate has 21.37% lesser buckling load with respect to the plate FH_NC_$(+45/-45)_{4s}$ under positive in-plane shear while it is 21.76% lesser in case of negative in-plane shear. In case of FH plates with big-sized cutouts, similar trend is observed with highest difference in buckling load with respect to the plate without cutout. Plate FH_D3_$(+45/-45)_{4s}$ has 34.61% lesser buckling load with respect to the plate FH_NC_$(+45/-45)_{4s}$ under positive in-plane shear while it is 36.21% lesser in case of negative in-plane shear as shown in Fig. 5.11. It is apparent that, as the size of cutout increases the critical buckling load decreases.

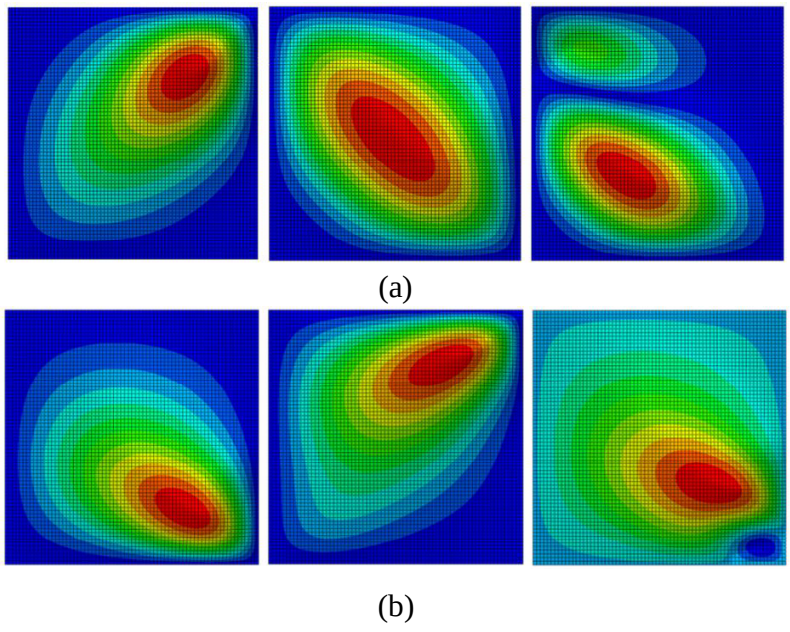

(a)

(b)

Fig. 5.5. Buckling mode shapes of functionally graded hybrid plates analyzed using numerical simulation under: (a) Positive in-plane shear load [Mode-I, II, III] (b) Negative in-plane shear load [Mode-I, II, III]

5.4.2. First ply failure load

The first ply failure load in all the plates is predicted by a tensor polynomial form of Tsai-Hill failure criterion incorporated in the numerical simulation. The first ply failure load values of all the FH plates analyzed are presented in Table 5.2. The plate with fiber aligned in (+45/-45) direction with and without cutouts is observed to have maximum first ply failure (FPF) load under positive in-plane shear load while it is observed to be higher in plates with fiber aligned in (+45/-45/0/90) direction under negative in-plane shear load. This signifies the effect of direction of applied shear load on the first ply failure load of functionally graded hybrid plates. Among the plates with cutouts, diamond shaped cutout with small-sized perforation performs better in terms of first ply failure. Similar trend has been observed in case of functionally graded hybrid plate with respect to the critical buckling loads. The first ply failure load values are also presented in their respective load vs. displacement plots of the plate for early instance. The specific effect of various parameters on buckling and first ply failure loads are further described in the following section.

5.4.3. Effect of direction of in-plane shear load

The maximum critical buckling and first ply failure loads are observed in functionally graded hybrid plates subjected to negative in-plane shear load. This is due to the alignment of compressive force in the fiber direction by the applied negative shear force. The compressive component of the applied negative shear load is acting along the 45^o fiber direction. Also, in the layup (+45/-45) stacking sequence, the bending stiffness coefficients D16, D26 enhances the negative shear buckling performance of the laminates. Therefore, critical buckling load of functionally graded hybrid laminated plates performs better in (+45/-45) layup sequence irrespective of cutout size and shape as shown in Figs. 5.9(a, b), 5.10(a, b) and 5.11(a, b). The same trend has been observed for first ply failure as presented in Table 5.2. It is worth noting that FH plates have high out-of-plane displacement under negative shear load than positive shear load as shown in Figs. 5.12(a–j), 5.13(a–j), and 5.14(a–j). This can also be observed in graphs showing the effect of shape of cutouts (Figs. 5.15–5.17) irrespective of layup sequence and cutout size. From Fig. 5.12, i.e., plates with (0/90) stacking sequence, it can be deduced that, though FH plates analyzed under negative in-plane shear has high critical buckling load, the ultimate failure load is maximum in FH plates analyzed under positive in-plane shear load. The similar trend is also observed in plates with (+45/-45/0/90) stacking sequence plates as shown in Fig. 5.14. From Fig. 5.15, it is apparent that out-of-

plane displacement corresponding to the applied load in FH plates under negative in-plane shear is higher compared to the positive in-plane shear loaded FH plates. This response is regardless of the cutout size which is evident from Figs. 5.16 and 5.17. Therefore, FH plates are structurally efficient in terms of strength under negative in-plane shear loads.

5.4.4. Effect of cutouts

As observed in tables and figures given earlier, FH plates without cutouts has the highest critical buckling load, while amongst FH plates with cutouts, diamond shaped cutout plate is observed to have highest critical buckling load irrespective of layup sequence as shown in Fig. 5.9(a). It is apparent that diamond shaped cutout plate has better buckling performance irrespective of in-plane shear directions as shown in Fig. 5.9(a) and (b). From Figs. 5.9–5.11, it is evident that FH plate with diamond shaped cutout outperforms in case of all sized cutouts such as small, medium , and big. It is also observed that FH plates with elliptical cutout aligned horizontally (EH) and vertically (EV) have approximately similar buckling values in all the cases such as different sized cutouts, layup sequences, and applied in-plane shear loading directions. In case of size of cutouts, all FH plates having small-sized cutouts perform better in terms of critical buckling load, first ply failure load, and ultimate load carrying capacity as shown in Figs. 5.12–5.14. It is noteworthy that as the size of cutout increases, buckling load and stiffness of the material decrease as observed from the load vs. displacement plots (Figs. 5.12–5.14).

Table 5.2. First ply failure loads of functionally graded hybrid plates with fiber aligned in $(0/90)_{4s}$, $(-45/+45)_{4s}$, and $(-45/+45/0/90)_{2s}$ directions with and without cutouts

Specimen ID / Orientation	First ply failure load (kN)		
	$(0/90)_{4s}$	$(-45/+45)_{4s}$	$(-45/+45/0/90)_{2s}$
FH_NC	11.36	6.43	9.50
FH_C1	10.47	6.22	9.89
FH_C2	8.95	5.62	8.84
FH_C3	7.94	4.90	7.76
FH_D1	10.52	5.56	9.37
FH_D2	9.26	6.13	9.05
FH_D3	8.74	6.44	8.55

FH_EH1	9.46	6.16	9.44
FH_EH2	8.11	5.54	9.02
FH_EH3	7.28	4.77	6.10
FH_EV1	9.36	5.94	9.23
FH_EV2	8.67	5.53	8.92
FH_EV3	6.62	4.81	6.07
FH_S1	9.44	6.14	9.81
FH_S2	8.91	5.45	8.66
FH_S3	6.78	4.76	7.39

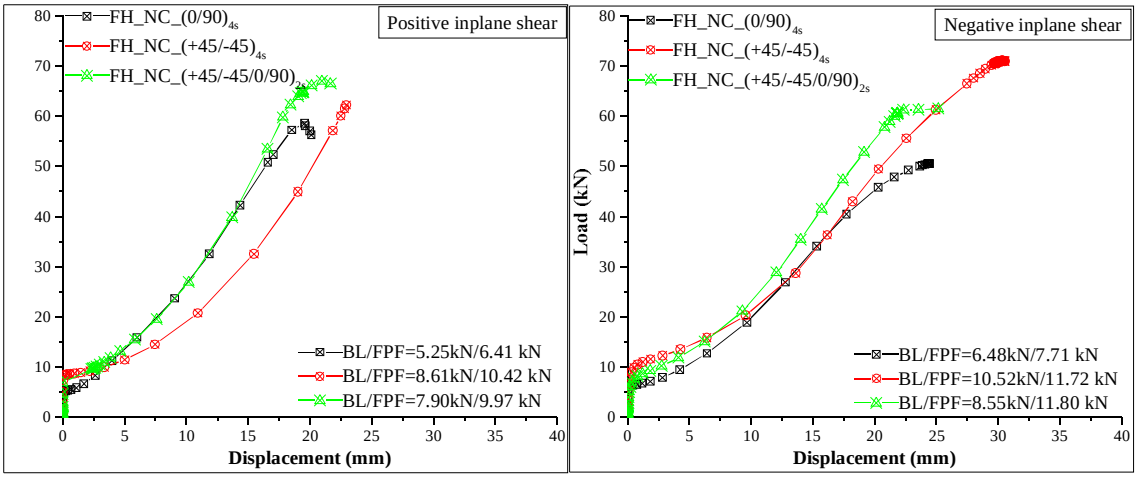

(a) (b)

Fig. 5.6. Load vs. displacement plots of functionally graded hybrid composite plates with fiber aligned in (0/90), (+45/-45), and (+45/-45/0/90) directions subjected to (a) Positive in-plane shear load (b) Negative in-plane shear load

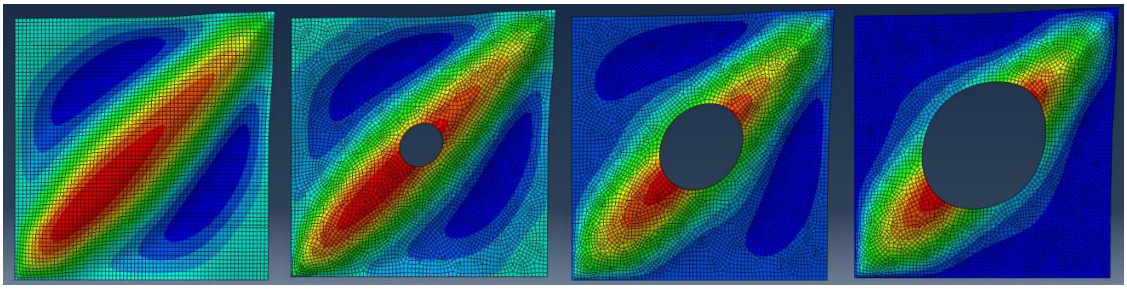

(a) (b) (c) (d)

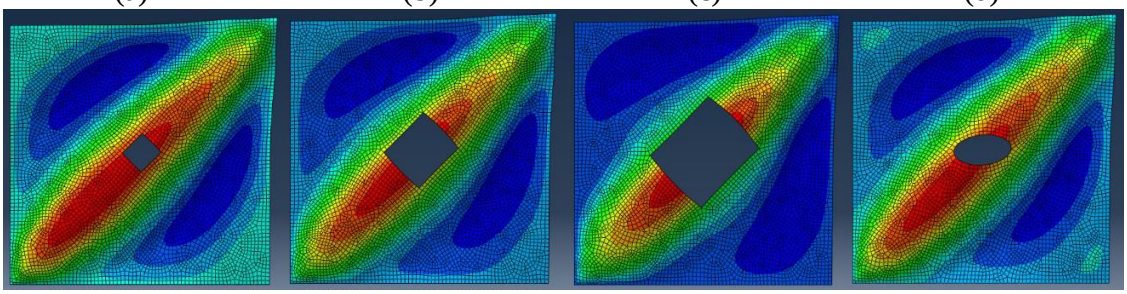

(e) (f) (g) (h)

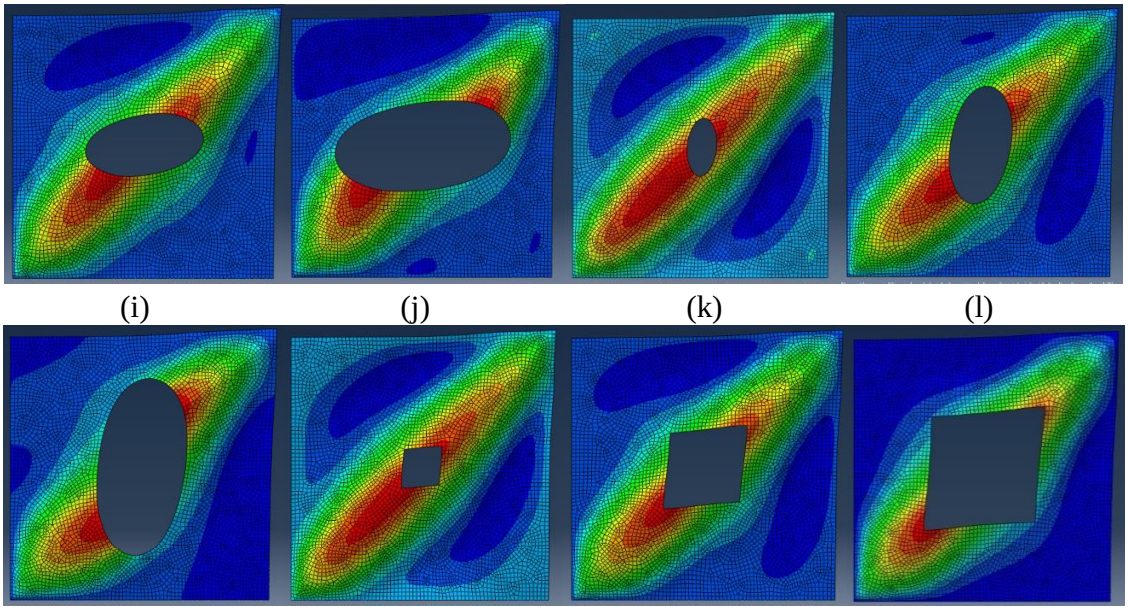

(i) (j) (k) (l)

(m) (n) (o) (p)

Fig. 5.7. Failure modes of FH plates with and without cutouts positive in-plane shear: (a) FH_NC (b) FH_C1 (c) FH_C2 (d) FH_C3 (e) FH_D1 (f) FH_D2 (g) FH_D3 (h) FH_EH1 (i) FH_EH2 (j) FH_EH3 (k) FH_EV1 (l) FH_EV2 (m) FH_EV3 (n) FH_S1 (o) FH_S2 (p) FH_S3

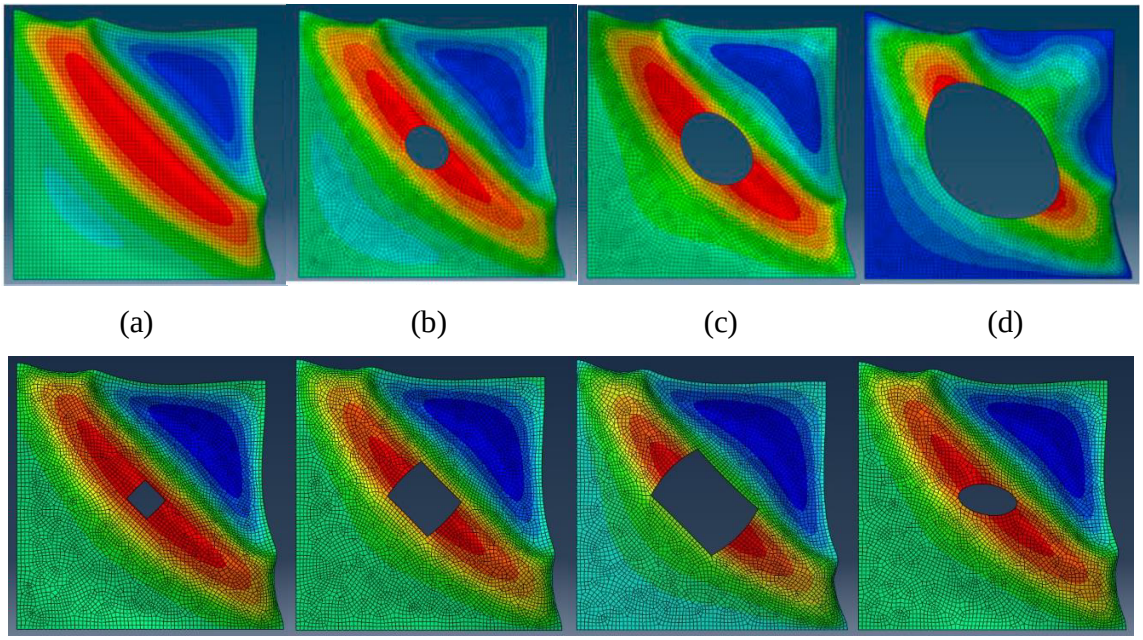

(a) (b) (c) (d)

(e) (f) (g) (h)

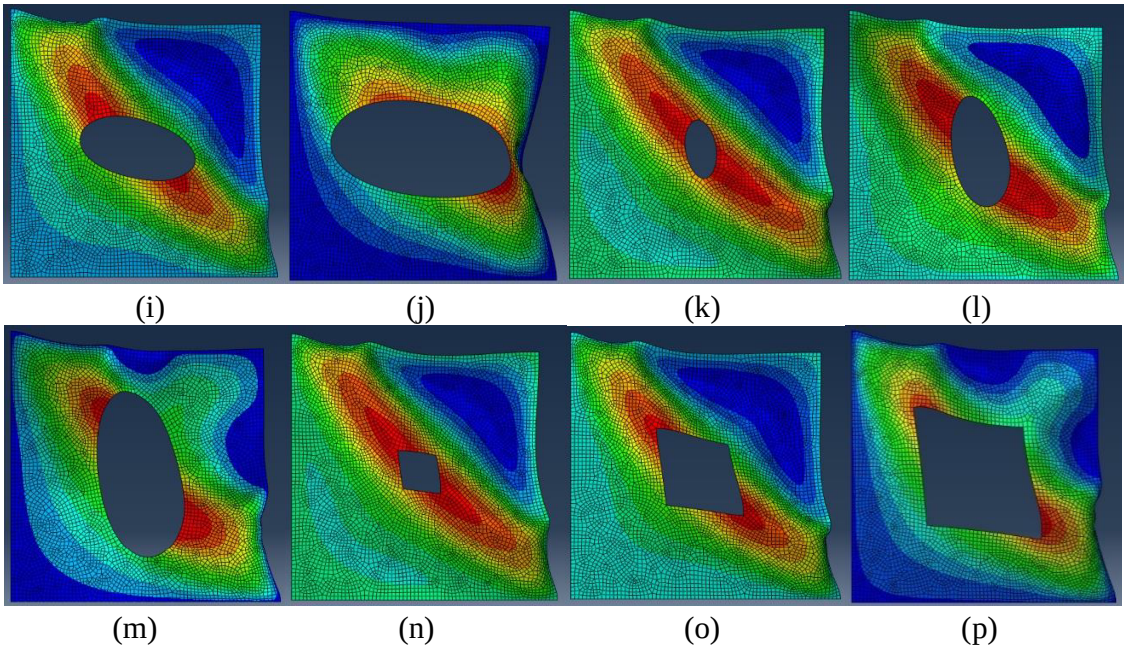

Fig. 5.8. Failure modes of FH plates with and without cutouts under negative in-plane shear: (a) FH_NC (b) FH_C1 (c) FH_C2 (d) FH_C3 (e) FH_D1 (f) FH_D2 (g) FH_D3 (h) FH_EH1 (i) FH_EH2 (j) FH_EH3 (k) FH_EV1 (l) FH_EV2 (m) FH_EV3 (n) FH_S1 (o) FH_S2 (p) FH_S3

5.4.5. Effect of stacking sequence

Fiber orientation in the plates is one of the significant parameters to be considered since the buckling response, failure, and strength also depends on it (Fig. 5.4). Irrespective of material type (i.e., plain CFRP, plain GFRP and FH plates), the plate with fiber aligned in (+45/- 45) direction has highest critical buckling load. The critical buckling loads of the FH plates with and without cutouts of size small, medium, and big for different stacking sequences shown in Figs. 5.9–5.11, respectively. It is clear that critical buckling load of plate with $(+45/-45)_{4s}$ stacking sequence is dominant with respect to the other stacking sequences such as $(0/90)_{4s}$ and $(+45/-45/0/90)_{2s}$. The load vs. displacement plots of functionally graded hybrid plates with fiber aligned in (0/90), (+45/-45), and (+45/-45/0/90) directions with different shaped cutouts having three various sized perforations are shown in Figs. 5.12–5.14, respectively.

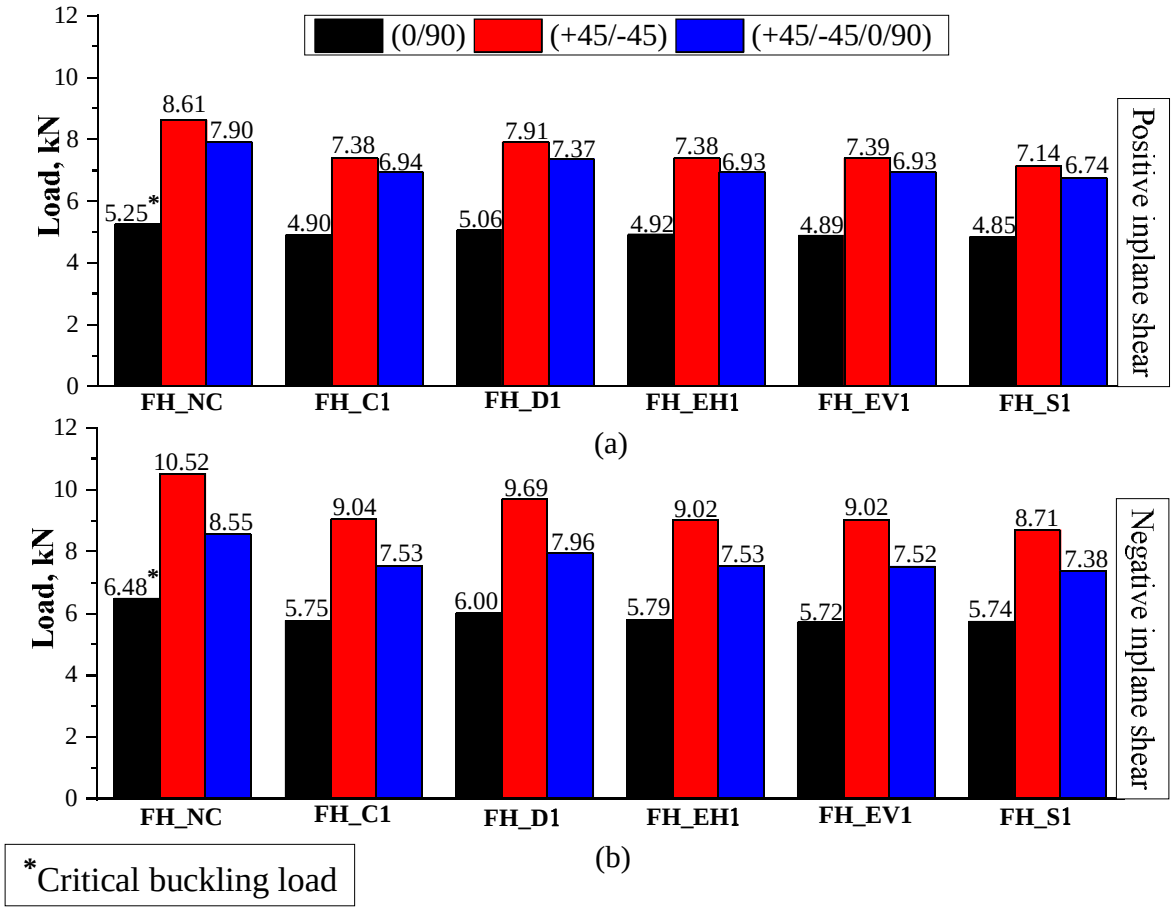

Fig. 5.9. Critical buckling loads of functionally graded hybrid (FH) composite plates with small sized cutouts with respect to FH composite plates without cutout subjected to (a) Positive in-plane shear load (b) Negative in-plane shear load

It is also observed that ultimate load carrying capacity is maximum in case of FH plates with fiber aligned in (+45/-45) direction subjected to negative in-plane shear load.-

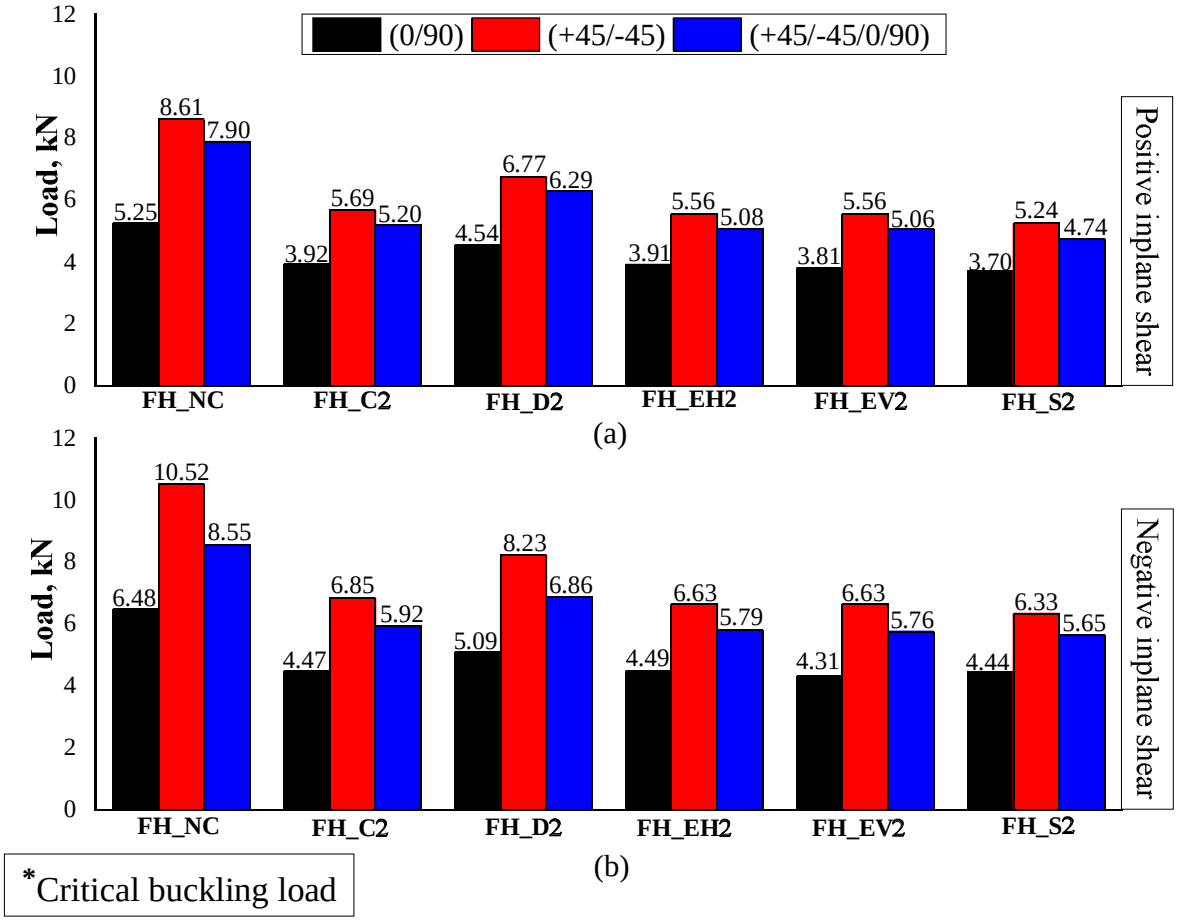

Fig. 5.10. Critical buckling loads of functionally graded hybrid (FH) composite plates with medium-sized cutouts with respect to FH composite plates without cutout subjected to (a) Positive in-plane shear load (b) Negative in-plane shear load

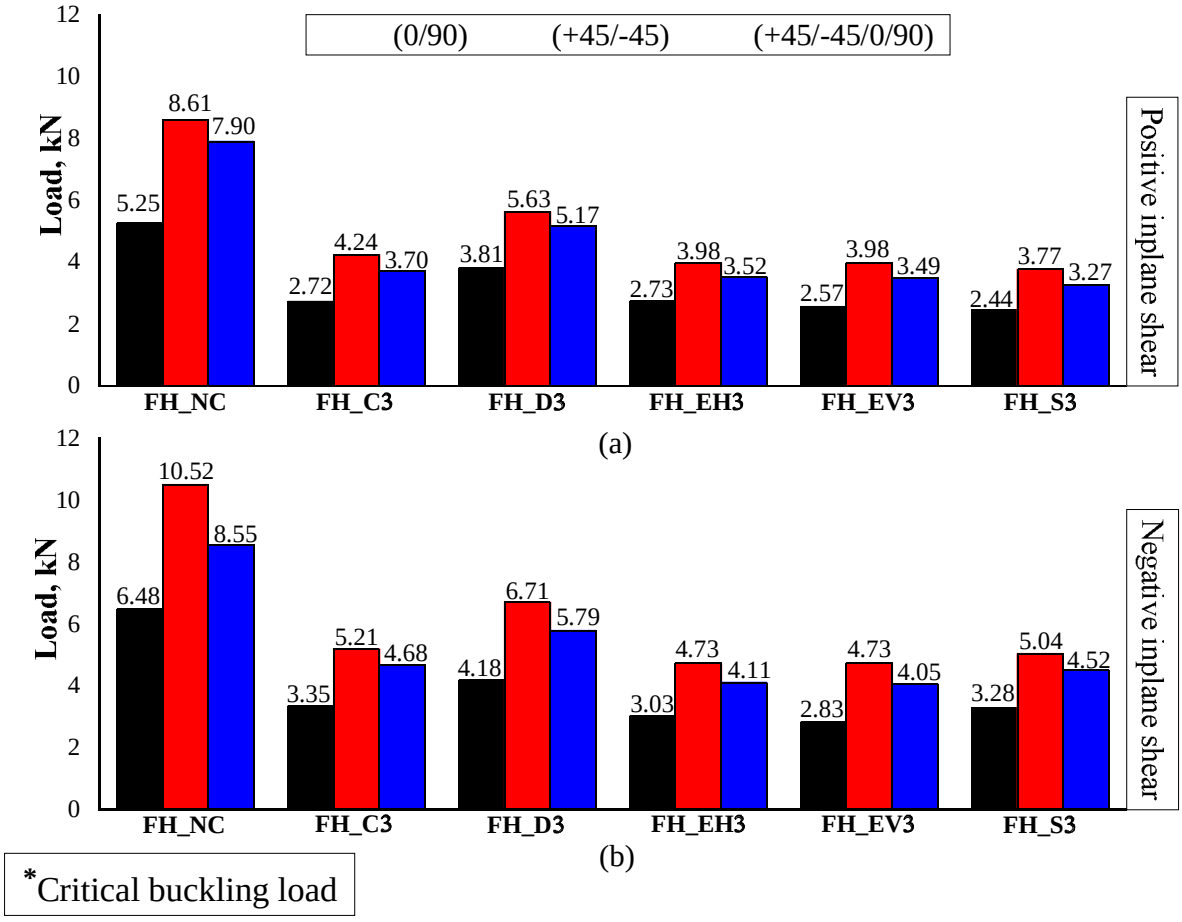

Fig. 5.11. Critical buckling loads of functionally graded hybrid (FH) composite plates with big-sized (big size) cutouts with respect to FH composite plates without cutout subjected to (a) Positive in-plane shear load (b) Negative in-plane shear load

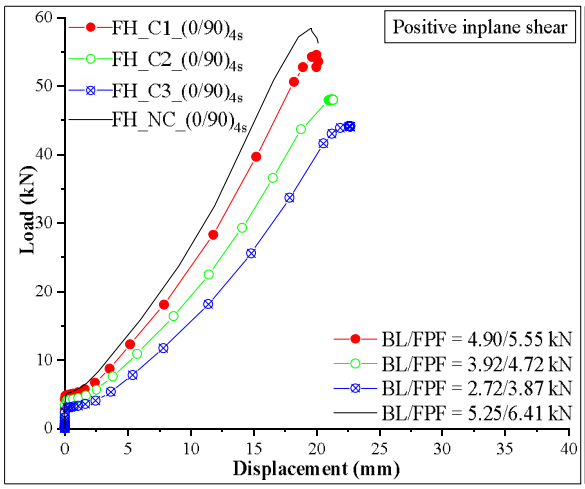
Positive inplane shear
FH_C1_(0/90)4s
FH_C2_(0/90)4s
FH_C3_(0/90)4s
FH_NC_(0/90)4s
BL/FPF = 4.90/5.55 kN
BL/FPF = 3.92/4.72 kN
BL/FPF = 2.72/3.87 kN
BL/FPF = 5.25/6.41 kN
Load (kN)
Displacement (mm)

(a)

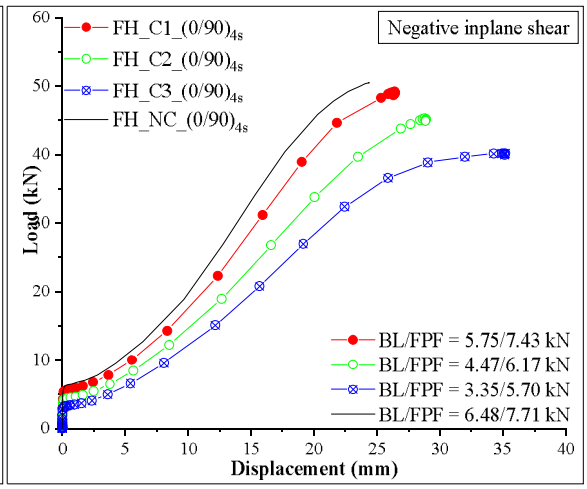
Negative inplane shear
FH_C1_(0/90)4s
FH_C2_(0/90)4s
FH_C3_(0/90)4s
FH_NC_(0/90)4s
BL/FPF = 5.75/7.43 kN
BL/FPF = 4.47/6.17 kN
BL/FPF = 3.35/5.70 kN
BL/FPF = 6.48/7.71 kN
Load (kN)
Displacement (mm)

(b)

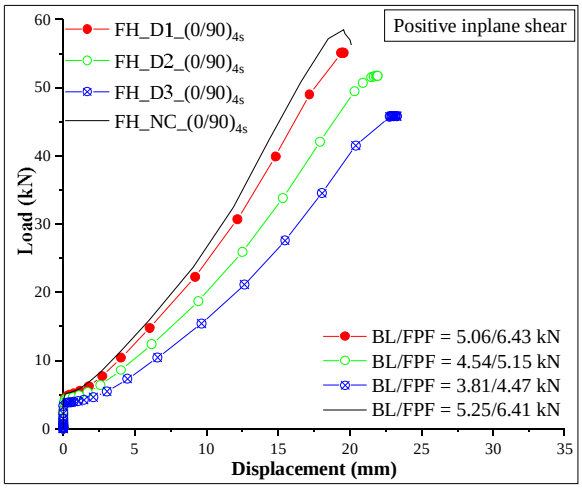
Positive inplane shear
FH_D1_(0/90)4s
FH_D2_(0/90)4s
FH_D3_(0/90)4s
FH_NC_(0/90)4s
BL/FPF = 5.06/6.43 kN
BL/FPF = 4.54/5.15 kN
BL/FPF = 3.81/4.47 kN
BL/FPF = 5.25/6.41 kN
Load (kN)
Displacement (mm)

(c)

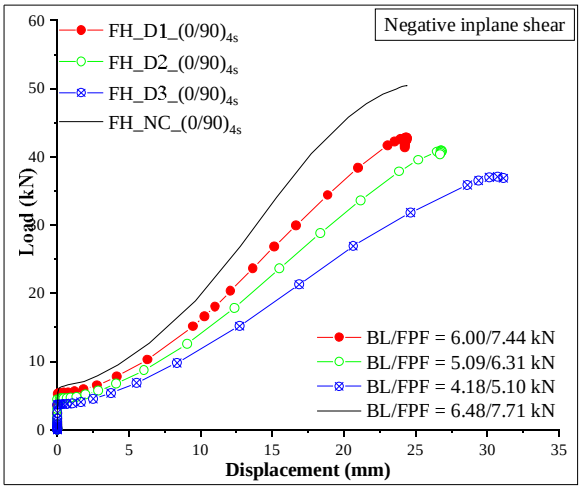
Negative inplane shear
FH_D1_(0/90)4s
FH_D2_(0/90)4s
FH_D3_(0/90)4s
FH_NC_(0/90)4s
BL/FPF = 6.00/7.44 kN
BL/FPF = 5.09/6.31 kN
BL/FPF = 4.18/5.10 kN
BL/FPF = 6.48/7.71 kN
Load (kN)
Displacement (mm)

(d)

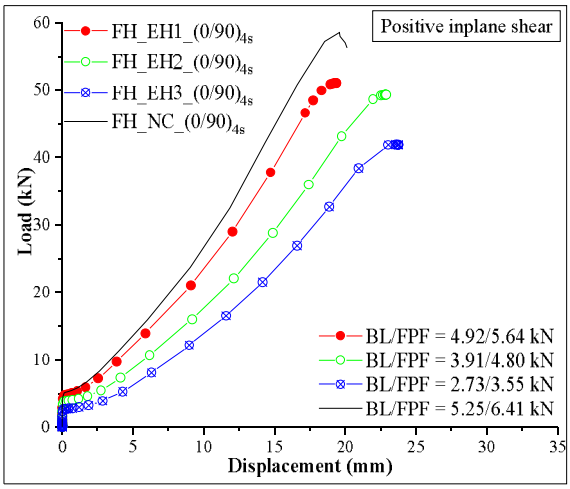
Positive inplane shear
FH_EH1_(0/90)4s
FH_EH2_(0/90)4s
FH_EH3_(0/90)4s
FH_NC_(0/90)4s
BL/FPF = 4.92/5.64 kN
BL/FPF = 3.91/4.80 kN
BL/FPF = 2.73/3.55 kN
BL/FPF = 5.25/6.41 kN
Load (kN)
Displacement (mm)

(e)

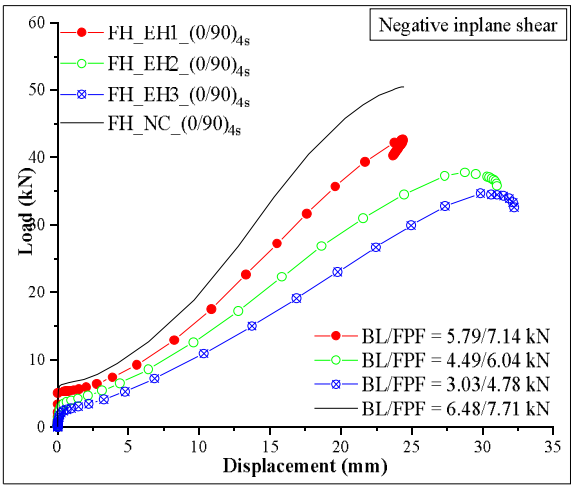
Negative inplane shear
FH_EH1_(0/90)4s
FH_EH2_(0/90)4s
FH_EH3_(0/90)4s
FH_NC_(0/90)4s
BL/FPF = 5.79/7.14 kN
BL/FPF = 4.49/6.04 kN
BL/FPF = 3.03/4.78 kN
BL/FPF = 6.48/7.71 kN
Load (kN)
Displacement (mm)

(f)

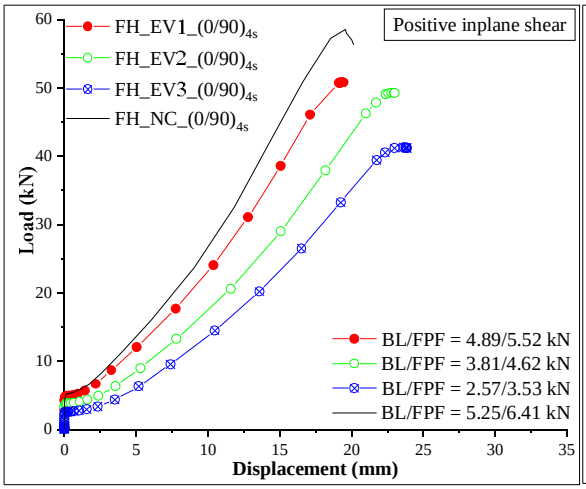
Positive inplane shear
FH_EV1_(0/90)4s
FH_EV2_(0/90)4s
FH_EV3_(0/90)4s
FH_NC_(0/90)4s
BL/FPF = 4.89/5.52 kN
BL/FPF = 3.81/4.62 kN
BL/FPF = 2.57/3.53 kN
BL/FPF = 5.25/6.41 kN
Load (kN)
Displacement (mm)

(g)

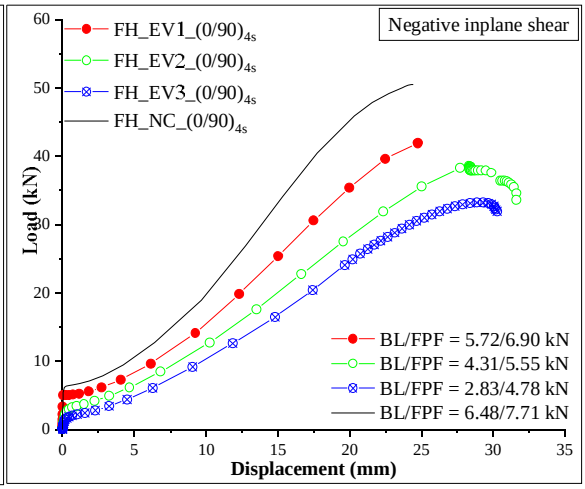
Negative inplane shear
FH_EV1_(0/90)4s
FH_EV2_(0/90)4s
FH_EV3_(0/90)4s
FH_NC_(0/90)4s
BL/FPF = 5.72/6.90 kN
BL/FPF = 4.31/5.55 kN
BL/FPF = 2.83/4.78 kN
BL/FPF = 6.48/7.71 kN
Load (kN)
Displacement (mm)

(h)

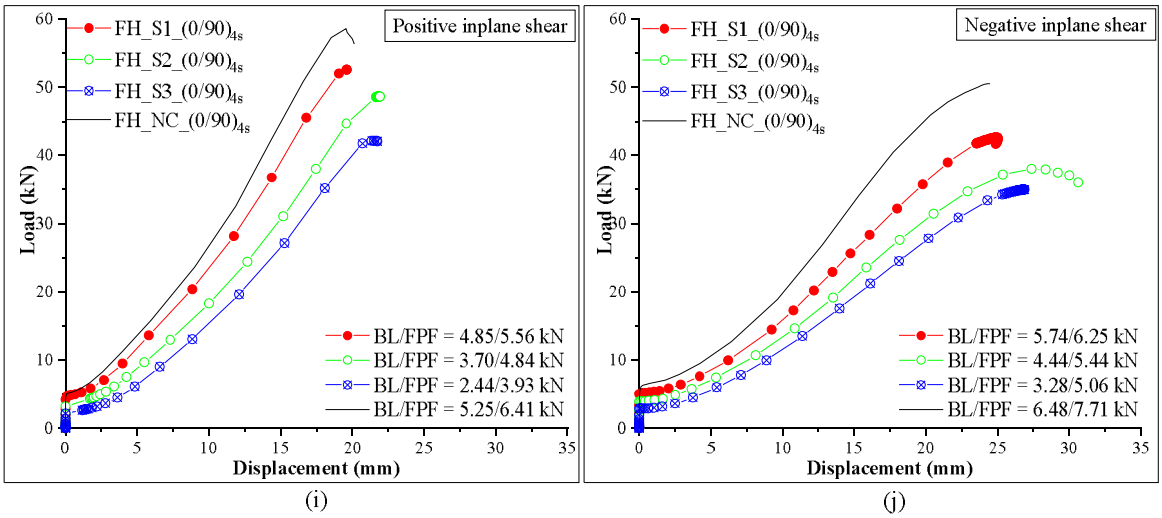

Fig. 5.12. Load vs. displacement plots of functionally graded hybrid plates with fiber aligned in (0/90) direction with different shaped and sized cutouts w.r.t. plate without cutout subjected to positive and negative in-plane shear load: (a) Circular shaped cutout under positive in-plane shear load (b) Circular cutout under negative in-plane shear load (c) Diamond shaped cutout under positive in-plane shear load (d) Diamond shaped cutout under negative in-plane shear load (e) Elliptical shaped cutout aligned horizontally under positive in-plane shear load (f) Elliptical shaped cutout aligned horizontally under negative in-plane shear load (g) Elliptical shaped cutout aligned vertically under positive in-plane shear load (h) Elliptical shaped cutout aligned vertically under negative in-plane shear load (i) Square shaped cutout under positive in-plane shear load (j) Square shaped cutout under negative in-plane shear load

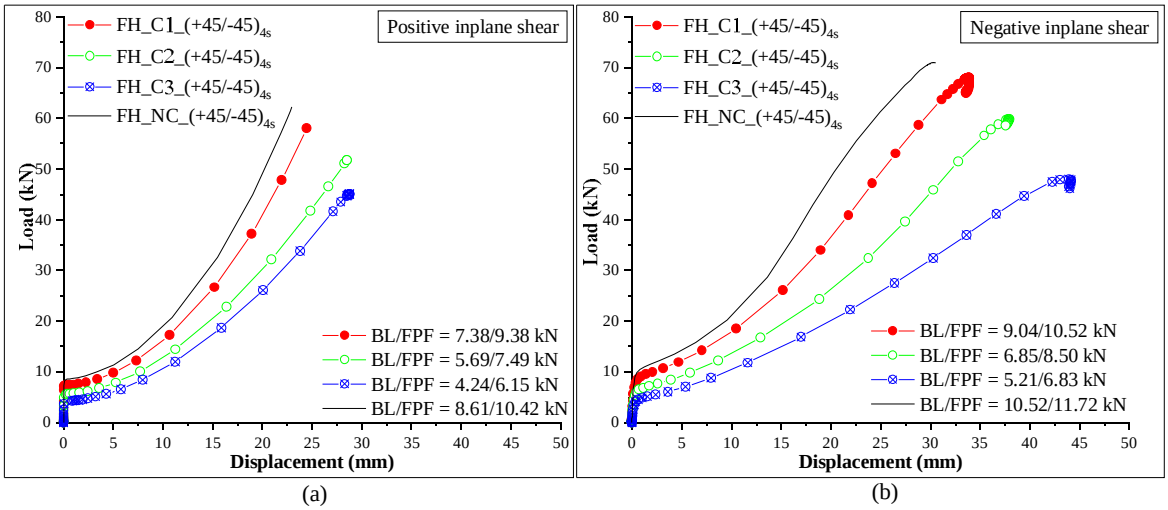

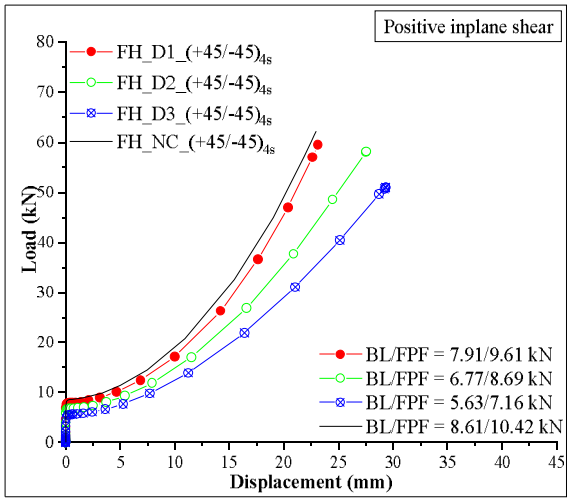
Positive inplane shear
FH_D1_(+45/-45)4s
FH_D2_(+45/-45)4s
FH_D3_(+45/-45)4s
FH_NC_(+45/-45)4s
BL/FPF = 7.91/9.61 kN
BL/FPF = 6.77/8.69 kN
BL/FPF = 5.63/7.16 kN
BL/FPF = 8.61/10.42 kN
Load (kN)
Displacement (mm)

(c)

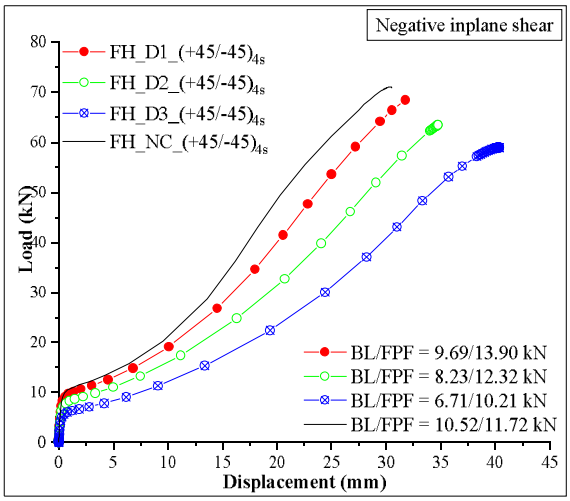
Negative inplane shear
FH_D1_(+45/-45)4s
FH_D2_(+45/-45)4s
FH_D3_(+45/-45)4s
FH_NC_(+45/-45)4s
BL/FPF = 9.69/13.90 kN
BL/FPF = 8.23/12.32 kN
BL/FPF = 6.71/10.21 kN
BL/FPF = 10.52/11.72 kN
Load (kN)
Displacement (mm)

(d)

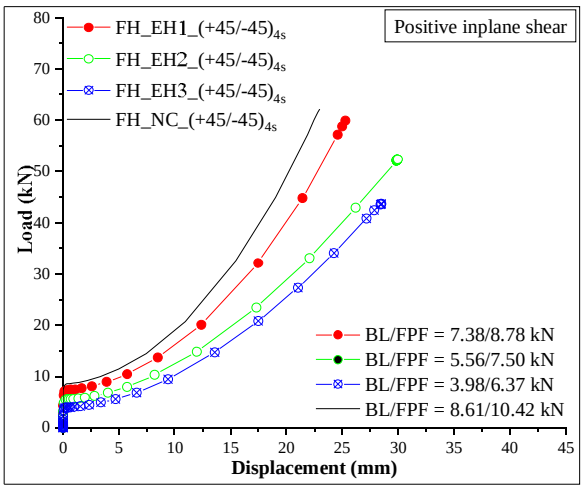
Positive inplane shear
FH_EH1_(+45/-45)4s
FH_EH2_(+45/-45)4s
FH_EH3_(+45/-45)4s
FH_NC_(+45/-45)4s
BL/FPF = 7.38/8.78 kN
BL/FPF = 5.56/7.50 kN
BL/FPF = 3.98/6.37 kN
BL/FPF = 8.61/10.42 kN
Load (kN)
Displacement (mm)

(e)

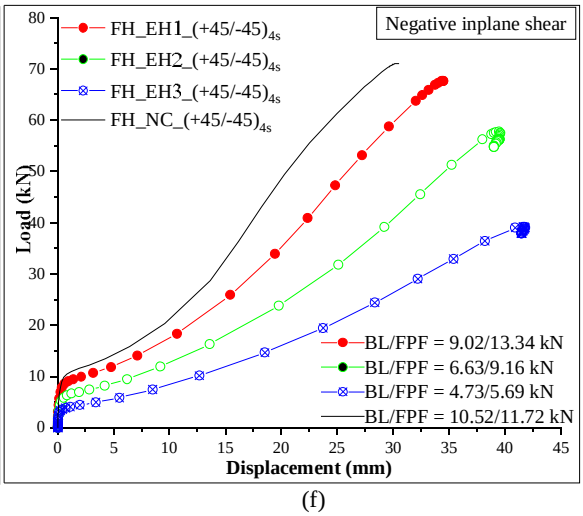
Negative inplane shear
FH_EH1_(+45/-45)4s
FH_EH2_(+45/-45)4s
FH_EH3_(+45/-45)4s
FH_NC_(+45/-45)4s
BL/FPF = 9.02/13.34 kN
BL/FPF = 6.63/9.16 kN
BL/FPF = 4.73/5.69 kN
BL/FPF = 10.52/11.72 kN
Load (kN)
Displacement (mm)

(f)

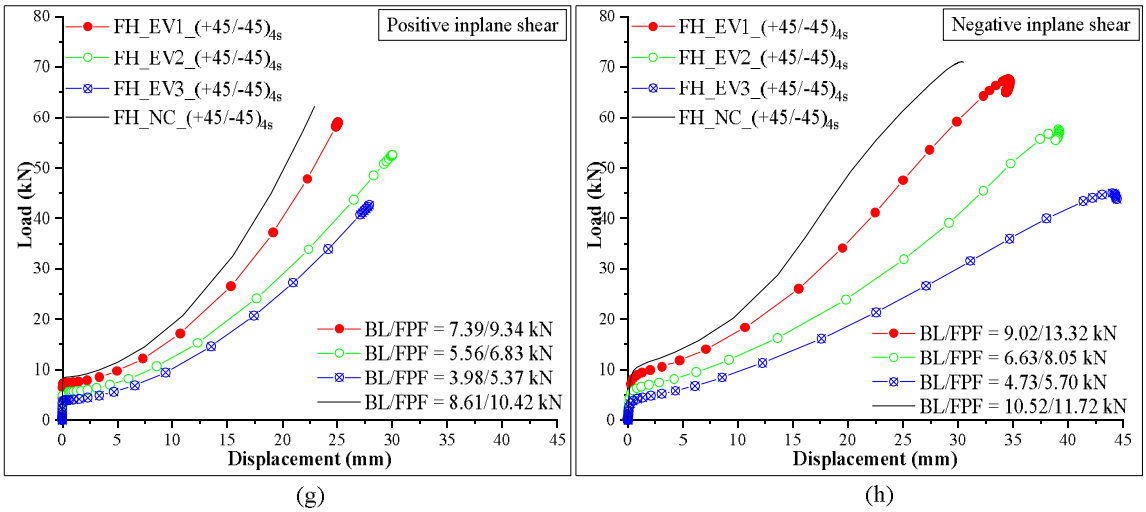

Fig. 5.13. Load vs. displacement plots of functionally graded hybrid plates with fiber aligned in (+45/-45) direction with different shaped and sized cutouts w.r.t. plate without cutout subjected to positive and negative in-plane shear load: (a) Circular shaped cutout under positive in-plane shear load (b) Circular cutout under negative in-plane shear load (c) Diamond shaped cutout under positive in-plane shear load (d) Diamond shaped cutout under negative in-plane shear load (e) Elliptical shaped cutout aligned horizontally under positive in-plane shear load (f) Elliptical shaped cutout aligned horizontally under negative in-plane shear load (g) Elliptical shaped cutout aligned vertically under positive in-plane shear load (h) Elliptical shaped cutout aligned vertically under negative in-plane shear load (i) Square shaped cutout under positive in-plane shear load (j) Square shaped cutout under negative in-plane shear load

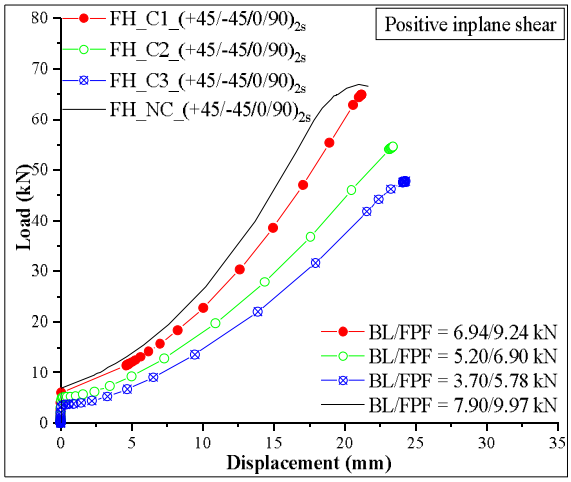
Positive inplane shear
FH_C1_(+45/-45/0/90)2s
FH_C2_(+45/-45/0/90)2s
FH_C3_(+45/-45/0/90)2s
FH_NC_(+45/-45/0/90)2s
BL/FPF = 6.94/9.24 kN
BL/FPF = 5.20/6.90 kN
BL/FPF = 3.70/5.78 kN
BL/FPF = 7.90/9.97 kN
Load (kN)
Displacement (mm)

(a)

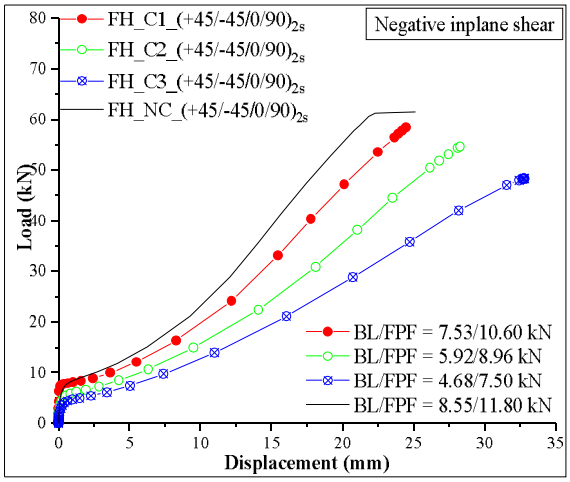
Negative inplane shear
FH_C1_(+45/-45/0/90)2s
FH_C2_(+45/-45/0/90)2s
FH_C3_(+45/-45/0/90)2s
FH_NC_(+45/-45/0/90)2s
BL/FPF = 7.53/10.60 kN
BL/FPF = 5.92/8.96 kN
BL/FPF = 4.68/7.50 kN
BL/FPF = 8.55/11.80 kN
Load (kN)
Displacement (mm)

(b)

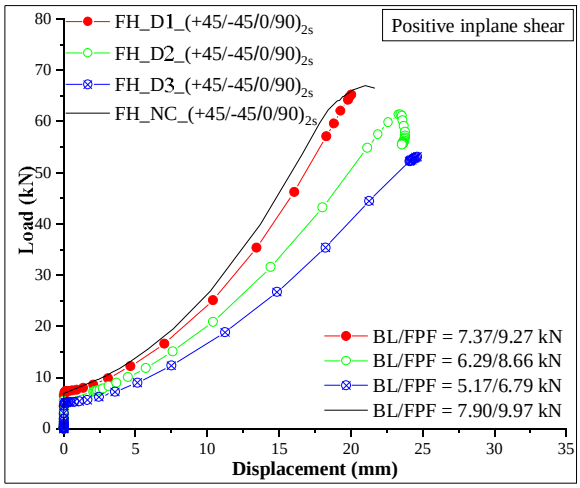
Positive inplane shear
FH_D1_(+45/-45/0/90)2s
FH_D2_(+45/-45/0/90)2s
FH_D3_(+45/-45/0/90)2s
FH_NC_(+45/-45/0/90)2s
BL/FPF = 7.37/9.27 kN
BL/FPF = 6.29/8.66 kN
BL/FPF = 5.17/6.79 kN
BL/FPF = 7.90/9.97 kN
Load (kN)
Displacement (mm)

(c)

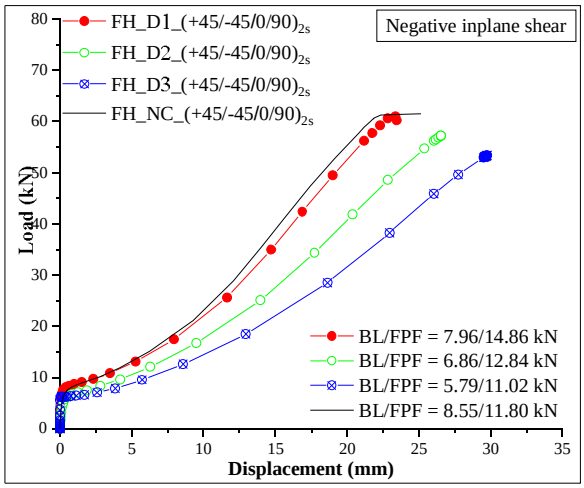
Negative inplane shear
FH_D1_(+45/-45/0/90)2s
FH_D2_(+45/-45/0/90)2s
FH_D3_(+45/-45/0/90)2s
FH_NC_(+45/-45/0/90)2s
BL/FPF = 7.96/14.86 kN
BL/FPF = 6.86/12.84 kN
BL/FPF = 5.79/11.02 kN
BL/FPF = 8.55/11.80 kN
Load (kN)
Displacement (mm)

(d)

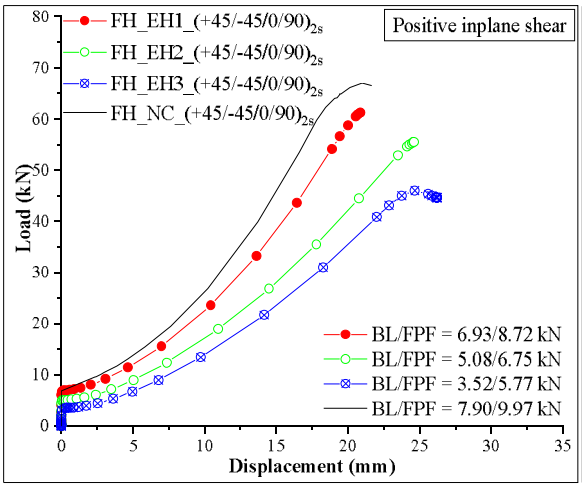
Positive inplane shear
FH_EH1_(+45/-45/0/90)2s
FH_EH2_(+45/-45/0/90)2s
FH_EH3_(+45/-45/0/90)2s
FH_NC_(+45/-45/0/90)2s
BL/FPF = 6.93/8.72 kN
BL/FPF = 5.08/6.75 kN
BL/FPF = 3.52/5.77 kN
BL/FPF = 7.90/9.97 kN
Load (kN)
Displacement (mm)

(e)

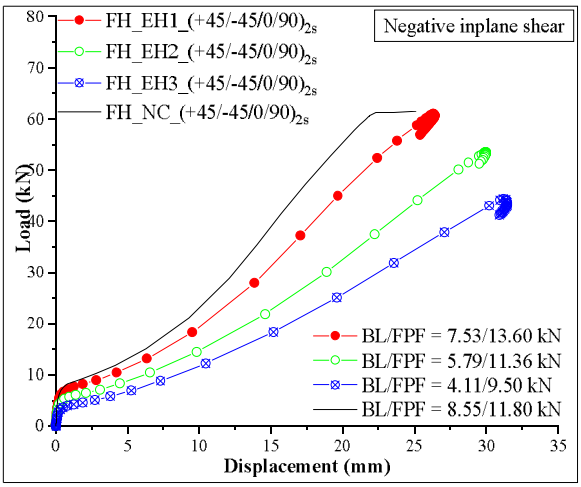
Negative inplane shear
FH_EH1_(+45/-45/0/90)2s
FH_EH2_(+45/-45/0/90)2s
FH_EH3_(+45/-45/0/90)2s
FH_NC_(+45/-45/0/90)2s
BL/FPF = 7.53/13.60 kN
BL/FPF = 5.79/11.36 kN
BL/FPF = 4.11/9.50 kN
BL/FPF = 8.55/11.80 kN
Load (kN)
Displacement (mm)

(f)

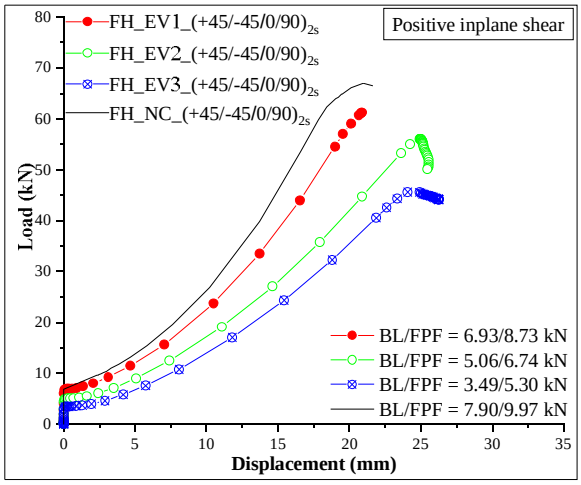
Positive inplane shear
FH_EV1_(+45/-45/0/90)2s
FH_EV2_(+45/-45/0/90)2s
FH_EV3_(+45/-45/0/90)2s
FH_NC_(+45/-45/0/90)2s
BL/FPF = 6.93/8.73 kN
BL/FPF = 5.06/6.74 kN
BL/FPF = 3.49/5.30 kN
BL/FPF = 7.90/9.97 kN
Load (kN)
Displacement (mm)

(g)

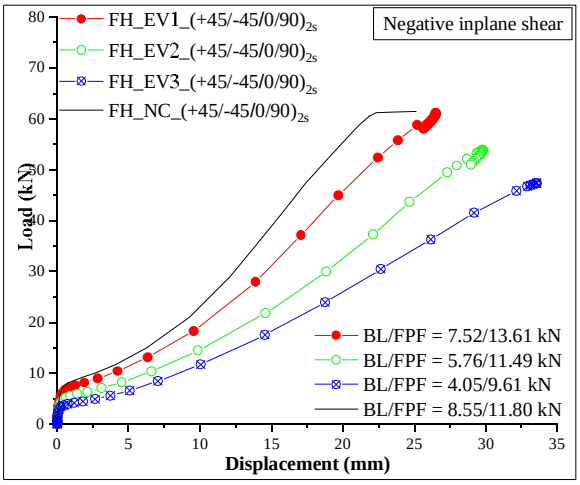
Negative inplane shear
FH_EV1_(+45/-45/0/90)2s
FH_EV2_(+45/-45/0/90)2s
FH_EV3_(+45/-45/0/90)2s
FH_NC_(+45/-45/0/90)2s
BL/FPF = 7.52/13.61 kN
BL/FPF = 5.76/11.49 kN
BL/FPF = 4.05/9.61 kN
BL/FPF = 8.55/11.80 kN
Load (kN)
Displacement (mm)

(h)

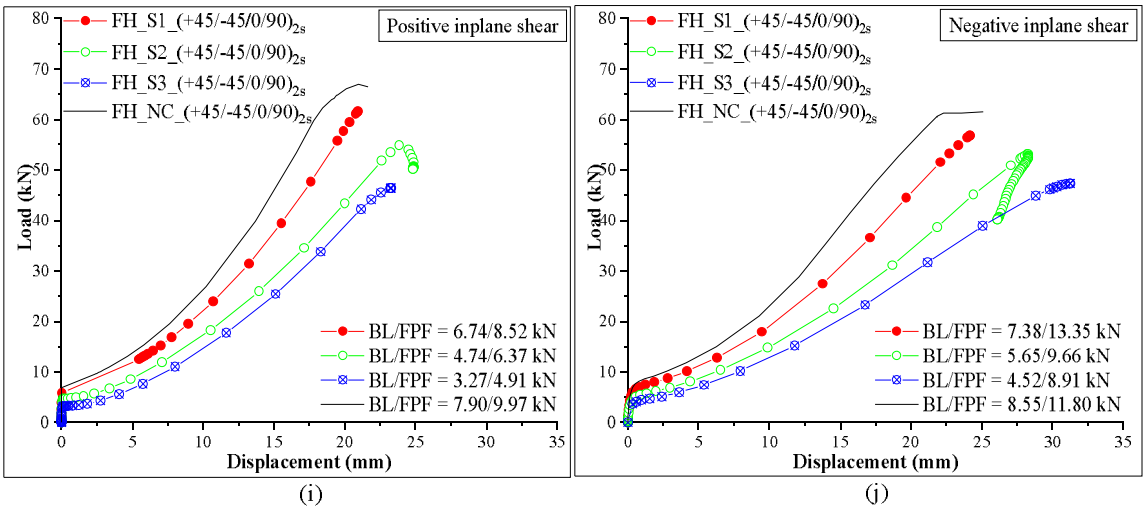

Fig. 5.14. Load vs. displacement plots of functionally graded hybrid plates with fiber aligned in (+45/-45/0/90) direction with different shaped and sized cutouts w.r.t. plate without cutout subjected to positive and negative in-plane shear load: (a) Circular shaped cutout under positive in-plane shear load (b) Circular cutout under negative in-plane shear load (c) Diamond shaped cutout under positive in-plane shear load (d) Diamond shaped cutout under negative in-plane shear load (e) Elliptical shaped cutout aligned horizontally under positive in-plane shear load (f) Elliptical shaped cutout aligned horizontally under negative in-plane shear load (g) Elliptical shaped cutout aligned vertically under positive in-plane shear load (h) Elliptical shaped cutout aligned vertically under negative in-plane shear load (i) Square shaped cutout under positive in-plane shear load (j) Square shaped cutout under negative in-plane shear load

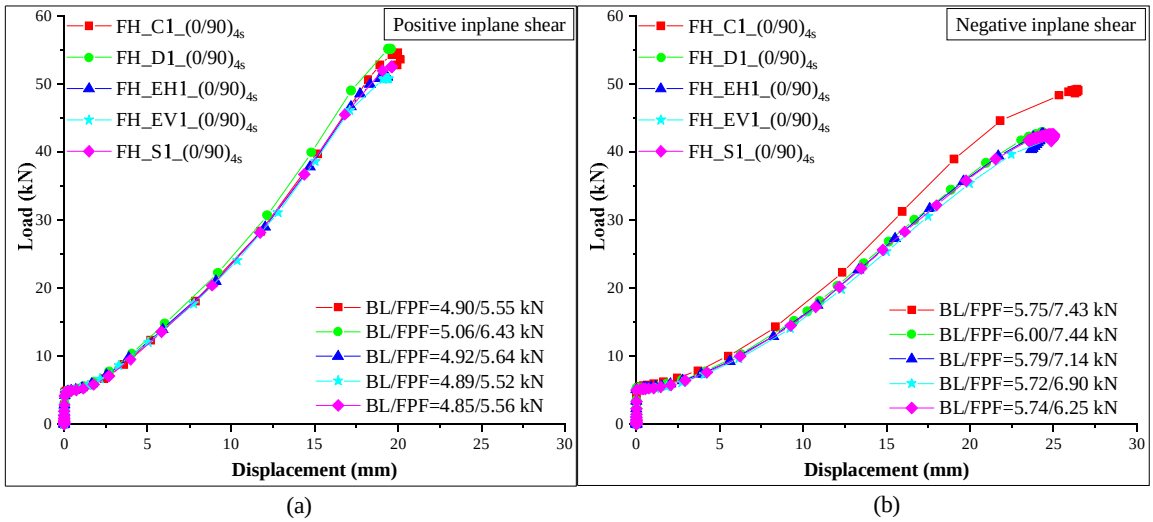

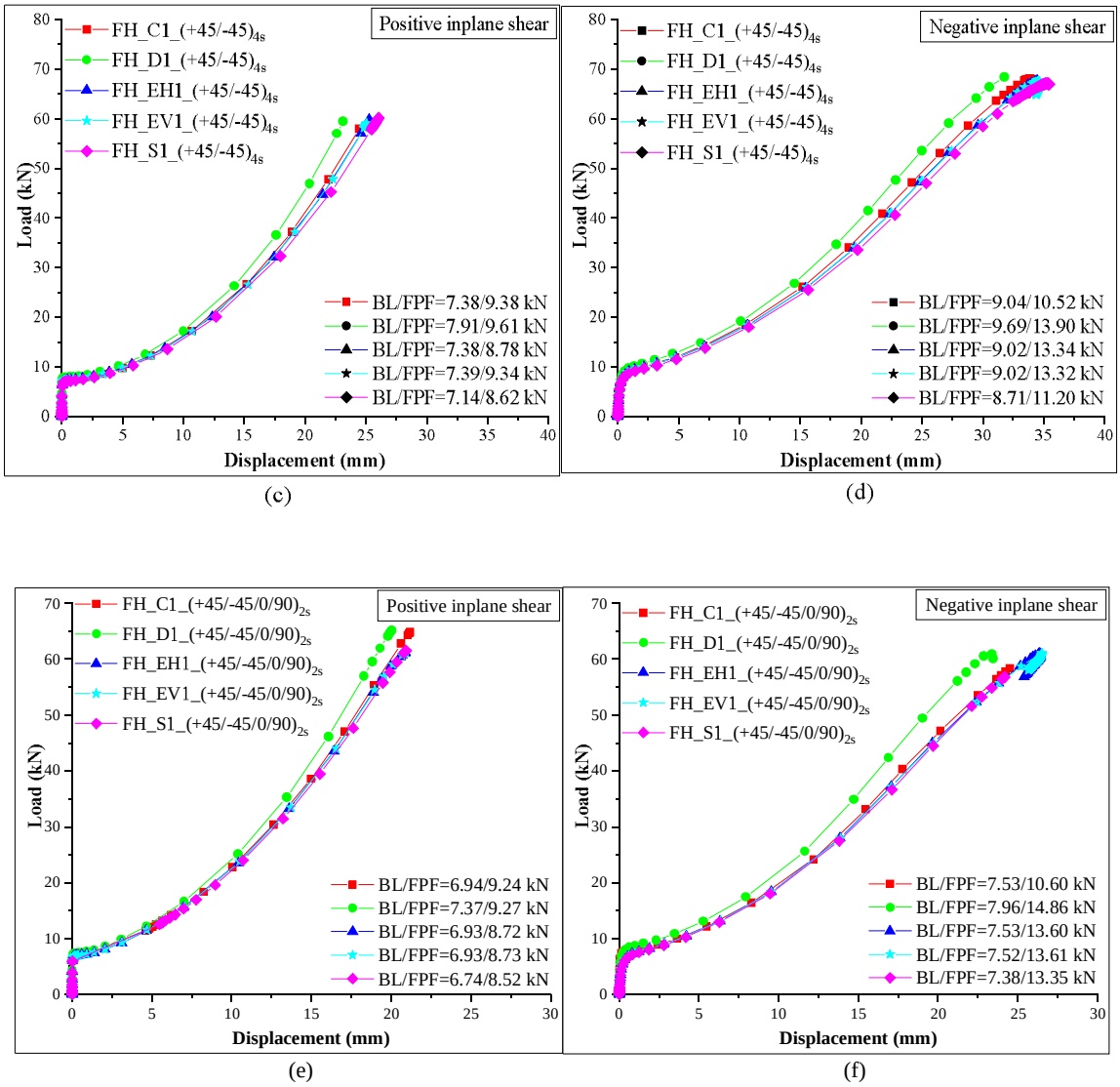

Fig. 5.15. Load vs. displacement plots of functionally graded hybrid plates subjected to both positive and negative shear loads with different shaped cutouts having small-sized cutout with fiber aligned in (a) (0/90) direction under positive in-plane shear load, (b) (0/90) direction under negative in-plane shear load, (c) (+45/-45) direction under positive in-plane shear load, (d) (+45/-45) direction under negative in-plane shear load, (e) (+45/-45/0/90) direction under positive in-plane shear load, and (f) (+45/-45/0/90) direction under negative in-plane shear load.

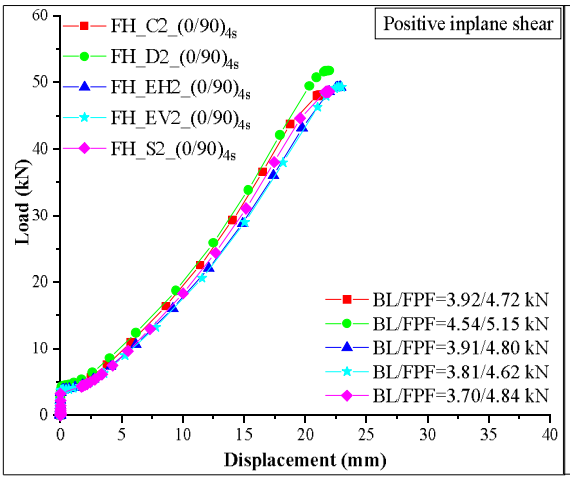
Positive inplane shear
FH_C2_(0/90)4s
FH_D2_(0/90)4s
FH_EH2_(0/90)4s
FH_EV2_(0/90)4s
FH_S2_(0/90)4s
BL/FPF=3.92/4.72 kN
BL/FPF=4.54/5.15 kN
BL/FPF=3.91/4.80 kN
BL/FPF=3.81/4.62 kN
BL/FPF=3.70/4.84 kN
Load (kN)
Displacement (mm)

(a)

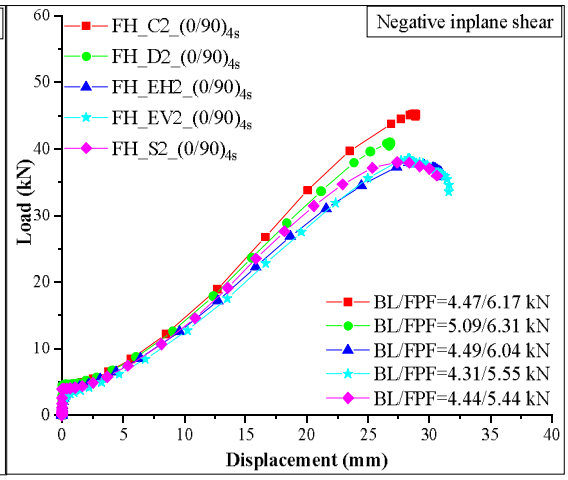
Negative inplane shear
FH_C2_(0/90)4s
FH_D2_(0/90)4s
FH_EH2_(0/90)4s
FH_EV2_(0/90)4s
FH_S2_(0/90)4s
BL/FPF=4.47/6.17 kN
BL/FPF=5.09/6.31 kN
BL/FPF=4.49/6.04 kN
BL/FPF=4.31/5.55 kN
BL/FPF=4.44/5.44 kN
Load (kN)
Displacement (mm)

(b)

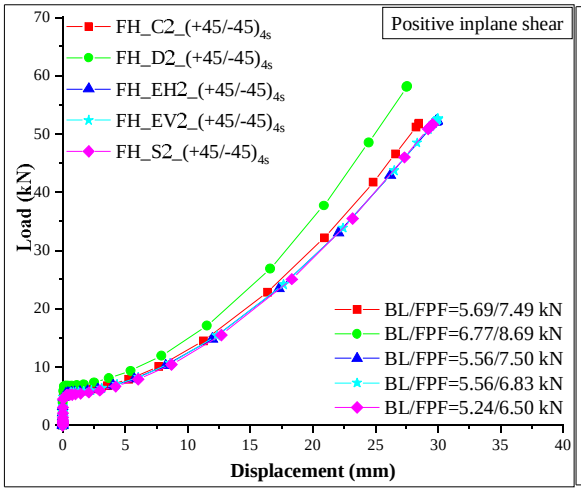
Positive inplane shear
FH_C2_(+45/-45)4s
FH_D2_(+45/-45)4s
FH_EH2_(+45/-45)4s
FH_EV2_(+45/-45)4s
FH_S2_(+45/-45)4s
BL/FPF=5.69/7.49 kN
BL/FPF=6.77/8.69 kN
BL/FPF=5.56/7.50 kN
BL/FPF=5.56/6.83 kN
BL/FPF=5.24/6.50 kN
Load (kN)
Displacement (mm)

(c)

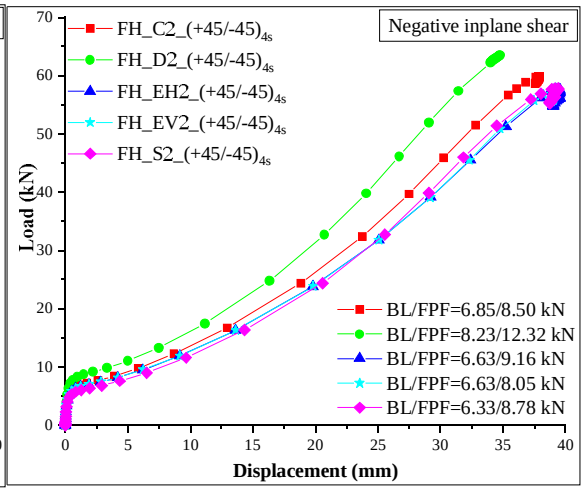
Negative inplane shear
FH_C2_(+45/-45)4s
FH_D2_(+45/-45)4s
FH_EH2_(+45/-45)4s
FH_EV2_(+45/-45)4s
FH_S2_(+45/-45)4s
BL/FPF=6.85/8.50 kN
BL/FPF=8.23/12.32 kN
BL/FPF=6.63/9.16 kN
BL/FPF=6.63/8.05 kN
BL/FPF=6.33/8.78 kN
Load (kN)
Displacement (mm)

(d)

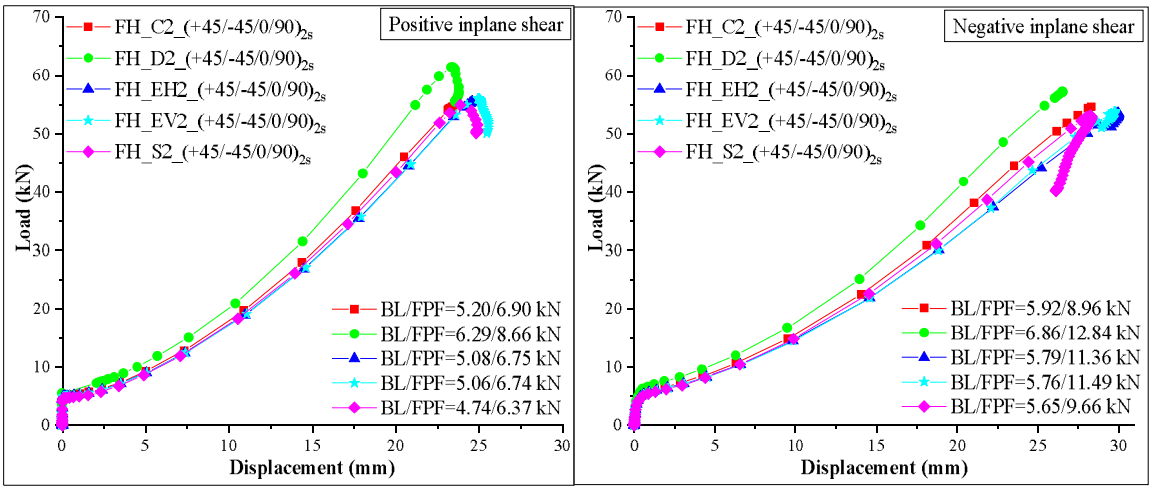

Fig. 5.16. Load vs. displacement plots of functionally graded hybrid plates subjected to both positive and negative shear loads with different shaped cutouts having 2-sized cutout with fiber aligned in (a) (0/90) direction under positive in-plane shear load, (b) (0/90) direction under negative in-plane shear load, (c) (+45/-45) direction under positive in-plane shear load, (d) (+45/-45) direction under negative in-plane shear load, (e) (+45/-45/0/90) direction under positive in-plane shear load, and (f) (+45/-45/0/90) direction under negative in-plane shear load.

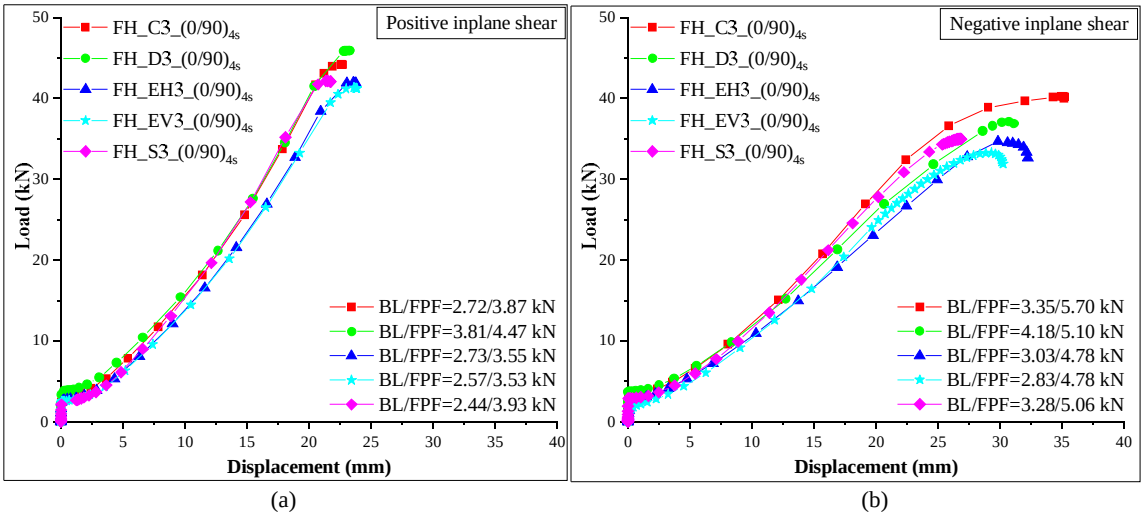

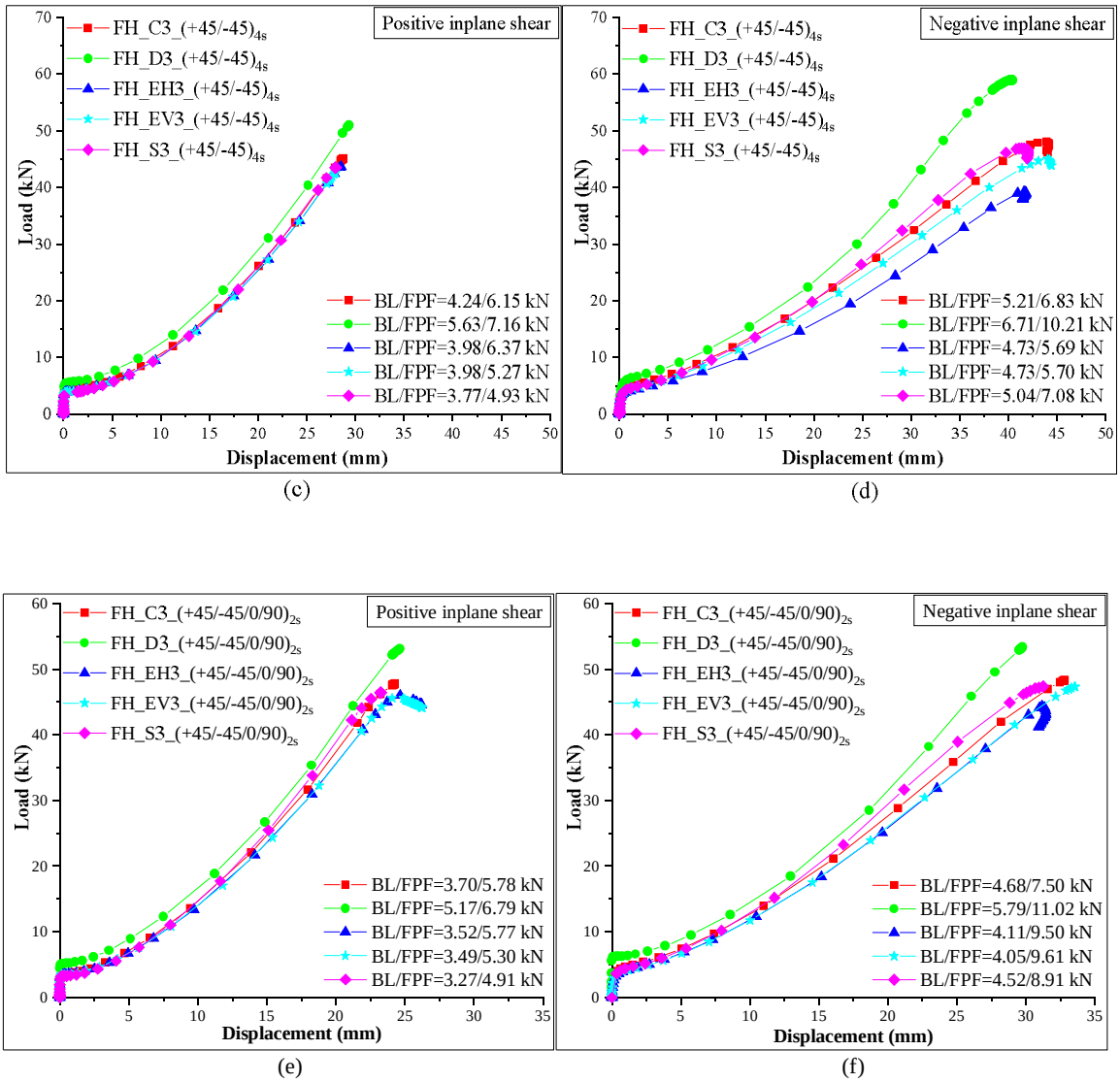

Fig. 5.17. Load vs. displacement plots of functionally graded hybrid plates subjected to both positive and negative shear loads with different shaped cutouts having big-sized cutout with fiber aligned in (a) (0/90) direction under positive in-plane shear load, (b) (0/90) direction under negative in-plane shear load, (c) (+45/-45) direction under positive in-plane shear load, (d) (+45/-45) direction under negative in-plane shear load, (e) (+45/-45/0/90) direction under positive in-plane shear load, and (f) (+45/-45/0/90) direction under negative in-plane shear load.

5.4.6. Effect of boundary conditions

The load vs deflection plots of previously published results from Kumar and Singh (2013) are validated with the ABAQUS software that has been used in the current study for numerical investigation. From Fig. 5.18, it can be observed that ABAQUS results are in good agreement with

the previously published results of Kumar and Singh (2013). This denotes the accuracy of the numerical tool used in the study. In Fig. 5.18 numerical validation of composite plates with flexural boundary conditions is carried out and the corresponding results are presented in Table 5.3. The difference in the published buckling load values and the numerical values obtained from ABAQUS is less than or equal to 1%. The first ply failure load of composite plates without cutouts with FBC1, FBC2, and FBC3 boundary conditions under positive shear occurred at deflections (w_{max}/h) 1.45, 1.43, and 1.31, respectively while the first ply failure load of composite plates under negative shear occurred at non-dimensional deflections (w_{max}/h) of 2.37, 1.94, and 1.65, respectively. The maximum and minimum first ply failure loads are observed in plates with FBC3 and FBC1 boundary conditions, respectively. It is worth notifying that as number of clamped edges increases in a plate, first ply failure load increase, corresponding deflection decreases. This trend is observed in composite plates with circular cutouts. The deflections observed in plates with circular cutouts with FBC1, FBC2, and FBC3 boundary conditions are 1.45, 1.43, and 1.31, respectively under positive shear and it is 2.37, 1.94, and 1.65, respectively under negative shear load.

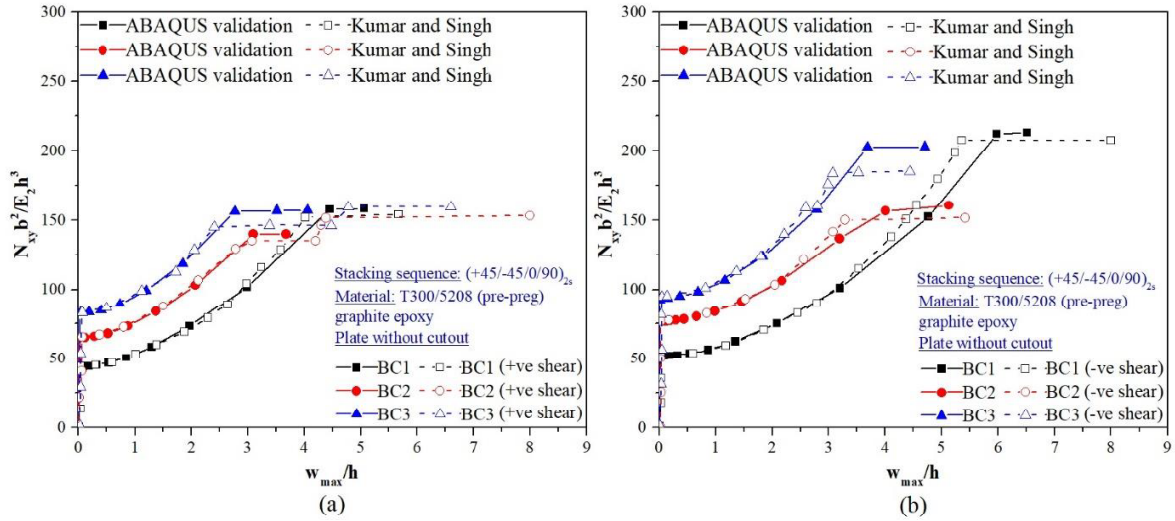

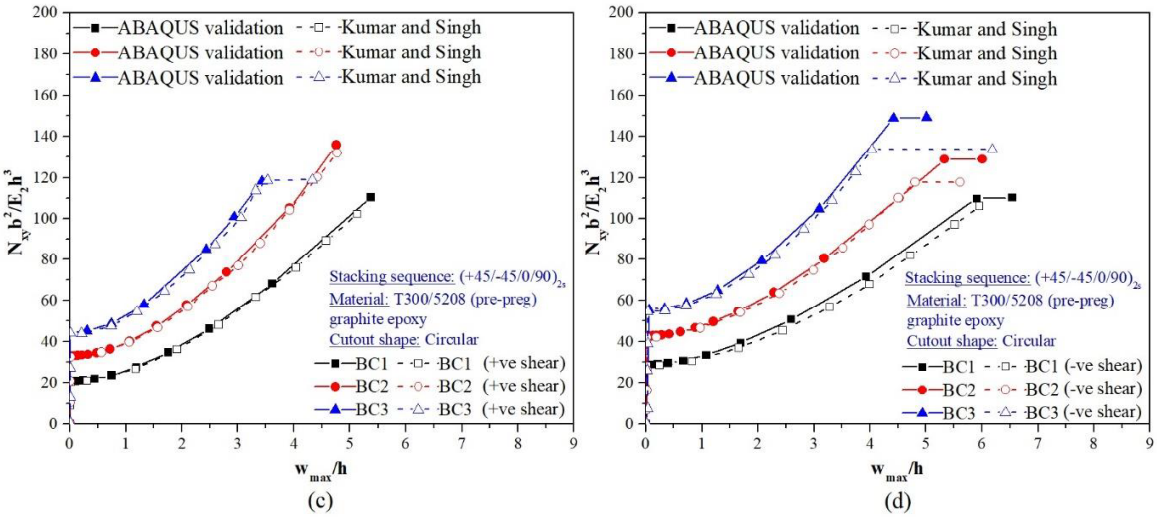

Note: BC1, BC2, BC3 are same as FBC1, FBC2, FBC3

Fig. 5.18. Validation of load-deflection response of quasi-isotropic laminate $(+45/-45/0/90)_{2s}$ with various flexural boundary conditions using ABAQUS with Kumar and Singh, 2013 under: (a) Positive in-plane shear load without cutout (b) Negative in-plane shear load without cutout (c) Positive in-plane shear load with circular cutout (d) Negative in-plane shear load with circular cutout

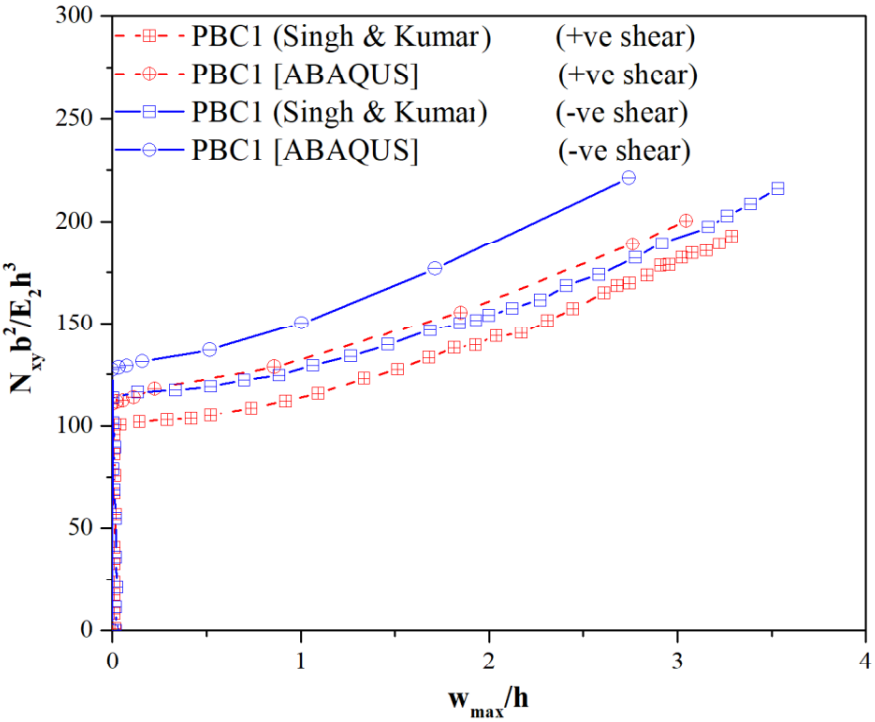

(a)

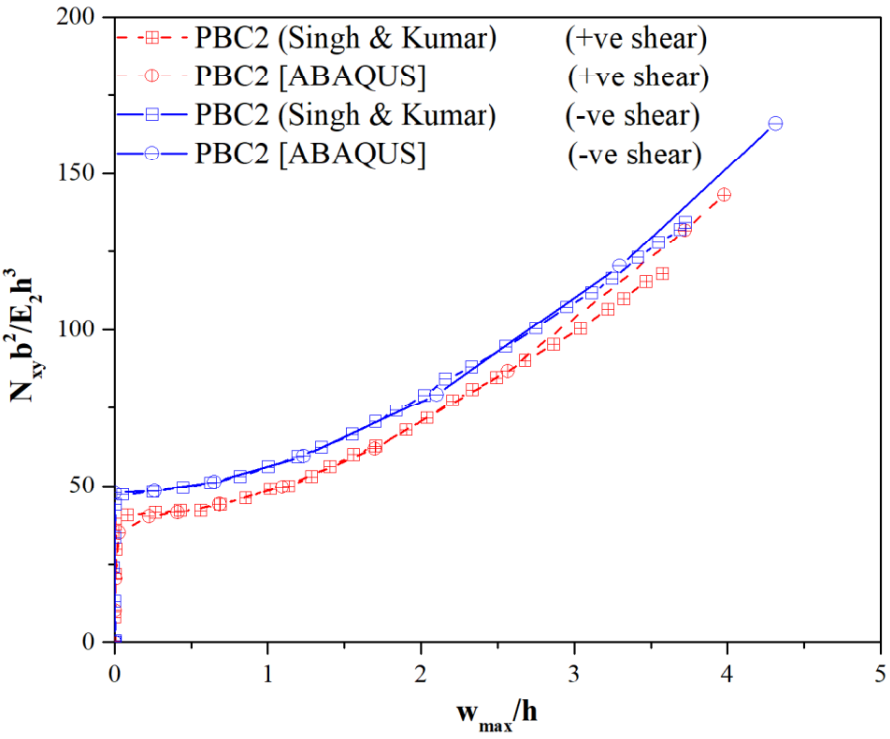
PBC2 (Singh & Kumar) (+ve shear)
PBC2 [ABAQUS] (+ve shear)
PBC2 (Singh & Kumar) (-ve shear)
PBC2 [ABAQUS] (-ve shear)
$N_{xy}b^2/E_2h^3$
w_{max}/h
0
50
100
150
200
0
1
2
3
4
5

(b)

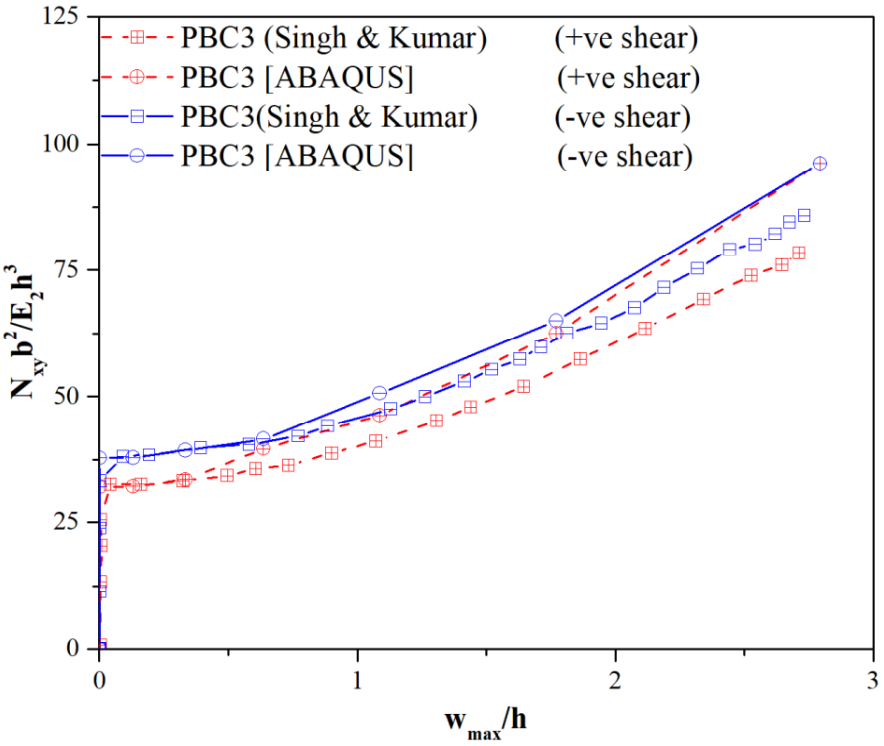
PBC3 (Singh & Kumar) (+ve shear)
PBC3 [ABAQUS] (+ve shear)
PBC3(Singh & Kumar) (-ve shear)
PBC3 [ABAQUS] (-ve shear)
$N_{xy}b^2/E_2h^3$
w_{max}/h
0
25
50
75
100
125
0
1
2
3

(c)

Fig. 5.19. Validation of load-deflection response of quasi-isotropic laminate $(+45/-45/0/90)_{2s}$ with various in-plane boundary conditions using ABAQUS with Singh and Kumar (2013) under positive and negative in-plane shear loads: (a) PBC1 (b) PBC2 (c) PBC3

Approximate non-dimensional deflection (w_{max}/h) values are obtained in the previously published research of Kumar and Singh (2013) as observed in Fig. 5.18 in the flexural boundary conditions case. In the event of in-plane boundary conditions, PBC1 boundary condition plates analyzed with ABAQUS has higher values than verified results while PBC2 and PBC3 boundary condition plates has closer values with respect to the published results of Singh and Kumar (1998) as observed in Fig. 5.19.

The buckling and failure load values of composite plates without and with circular cutout are presented in Table 5.3 and 5.4, respectively. The in-plane shear effects on composite laminates with different in-plane boundary restraints such as PBC1, PBC2, and PBC3 are shown in Fig. 5.20.

Table 5.3. Details of validated results using ABAQUS with the published data (Kumar and Singh, 2013) of composite plate without cutout with flexural boundary conditions

	FBC1 (without cutout)		FBC2 (without cutout)		FBC3 (without cutout)	
	(+ve shear)	(-ve shear)	(+ve shear)	(-ve shear)	(+ve shear)	(-ve shear)
ABAQUS BL♥/FPF♣/UL♠	43.6/61.6/158.1	51.5/87.1/213.0	64.6/90.1/140.0	76.4/93.0/160.5	82.3/98.3/157.0	92.8/116.5/203.0
Reference [20] BL♥/FPF♣/UL♠	43.7/61.4/151.4	51.2/82.0/207.5	65.4/87.0/150.4	77.0/101.4/149.8	83.7/102.7/159.7	94.2/119.0/183.9

♥Buckling load; ♣First-ply failure; ♠Ultimate failure load

Note: All the values are non-dimensional (i.e., $N_{xy}b^2/E_2h^3$) where, N_{xy} is In-plane shear load; b is width of the plate; E_2 is transverse modulus; h is thickness of the plate

Table 5.4. of composite plate with circular cutout with flexural boundary conditions

	FBC1 (circular cutout)		FBC2 (circular cutout)		FBC3 (circular cutout)	
	(+ve shear)	(-ve shear)	(+ve shear)	(-ve shear)	(+ve shear)	(-ve shear)
ABAQUS BL♥/FPF♣/UL♠	20.8/39.6/110.4	28.6/55.5/110.1	32.9/56.9/136.0	42.5/62.4/129.0	44.2/70.0/118.2	55.4/68.0/149.2
Reference [20] BL♥/FPF♣/UL♠	20.7/39.3/101.9	28.3/54.8/105.8	32.7/56.5/132.1	42.2/62.2/117.9	43.9/69.2/119.0	54.9/65.9/134.0

♥Buckling load; ♣First-ply failure; ♠Ultimate failure load

Note: All the values are non-dimensional (i.e., $N_{xy}b^2/E_2h^3$) where, N_{xy} is In-plane shear load; b is width of the plate; E_2 is transverse modulus; h is thickness of the plate

Table 5.5. Details of validated results using ABAQUS with the published data (Singh and Kumar, 1998) of composite plate without cutout with in-plane boundary conditions

	PBC1 (without cutout)		PBC2 (without cutout)		PBC3 (without cutout)	
	(+ve shear)	(-ve shear)	(+ve shear)	(-ve shear)	(+ve shear)	(-ve shear)
ABAQUS BL♥/FPF♣/UL♠	110.7/142.7/200.4	127.1/154.9/221.3	40.5/78.6/143.1	47.9/89.4/166.0	32.2/54.6/96.3	37.8/59.9/96.2
Reference [12] BL♥/FPF♣/UL♠	101.4/138.1/192.8	116.2/148.6/217.0	40.4/80.0/117.3	47.9/88.6/135.1	32.6/58.9/82.2	38.3/61.8/85.1

♥Buckling load; ♣First-ply failure; ♠Ultimate failure load

Note: All the values are non-dimensional (i.e., $N_{xy}b^2/E_2h^3$) where, N_{xy} is In-plane shear load; b is width of the plate; E_2 is transverse modulus; h is thickness of the plate

These results are validated numerically with ABAQUS software and the load-deflection responses of boundary conditions PBC1, PBC2, and PBC3 are presented in Figs. 5.19(a), 5.19(b), and 5.19(c), respectively and the corresponding load values are presented in Table 5.5. In case of PBC1 boundary condition, the buckling load values of published results is 9% lower than ABAQUS validated results while it is less than 1.3% in case of PBC2 and PBC3 boundary conditions. Though there is a considerable difference in values of PBC1 boundary conditions, the postbuckling path of both the curves are parallel as shown in Fig. 5.19(a). The maximum and minimum buckling and postbuckling strengths are observed in composite plates with PBC1 and PBC3 boundary conditions as shown in Table 5.5. The first ply failure loads of PBC1, PBC2, and PBC3 occurrs at non-dimensional deflection (w_{max}/h) of 1.38, 2.28, and 1.44 deflections under positive shear load and it is 1.13, 2.40, and 1.52 deflections under negative shear load. It is worth notifying that the first ply failure load of composite plate with PBC2 boundary condition occurrs at greater deflection amongst other boundary conditions, i.e., PBC1 and PBC3.

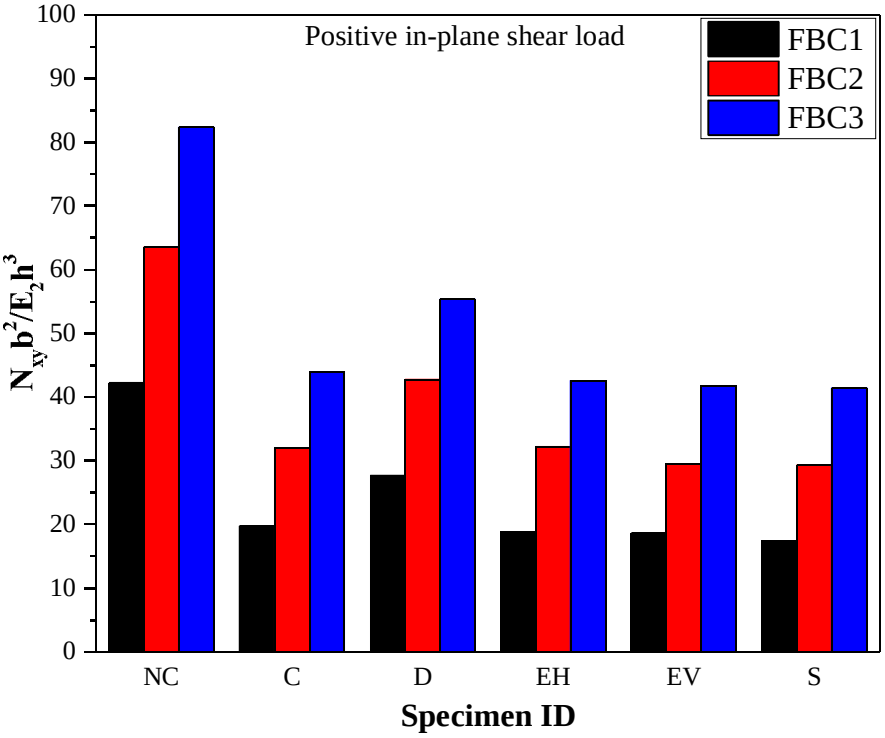

(a)

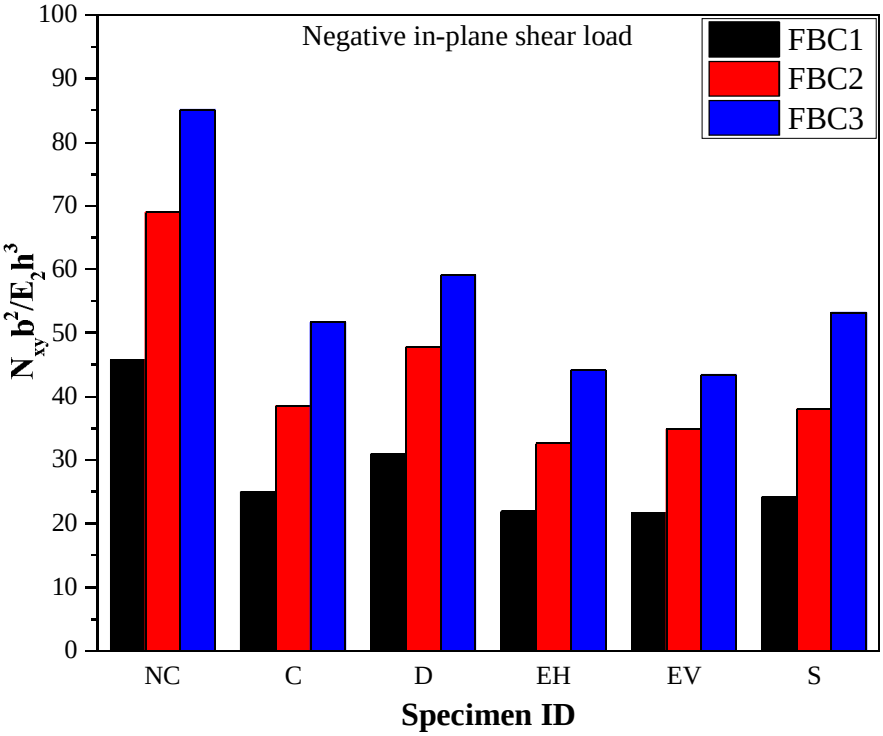

(b)

Fig. 5.20. Critical buckling loads of functionally graded hybrid composite plates aligned in $(+45/-45/0/90)_{2s}$ direction with and without cutouts under: (a) Positive in-plane shear; (b) Negative in-plane shear

This observation is similar in case of ultimate failure load of plate with PBC2 boundary condition as shown in Fig. 5.19(b). Therefore, the numerical results are in good agreement with the published results, hence, on the basis of accuracy of the software, functionally graded hybrid composite plates with different flexural and in-plane boundary conditions have been studied under in-plane shear loading (both positive and negative in plane shear) and results are described below.

The boundary conditions parameter is considered to check their effect on postbuckling response. Initially critical buckling loads are evaluated for FH plates with various flexural boundary conditions, i.e., FBC1, FBC2 and FBC3 as shown in Fig. 5.20. It is observed that FBC1 boundary condition i.e., plate simply supported on all four edges has less critical buckling load value while FBC3 boundary condition, i.e., plates clamped on all four edges has higher critical buckling load value irrespective of the directions of applied shear load. Among the FH plates with cutouts, diamond shaped cutout plate has maximum critical buckling load irrespective of the type of

flexural boundary condition and direction of applied shear loads as shown in Figs. 5.20(a) and 5.20(b).

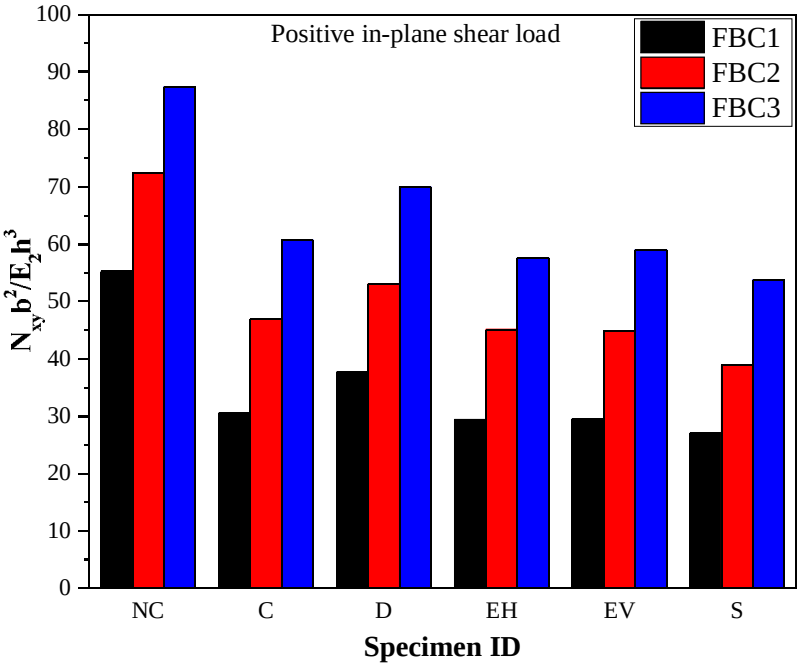

(a)

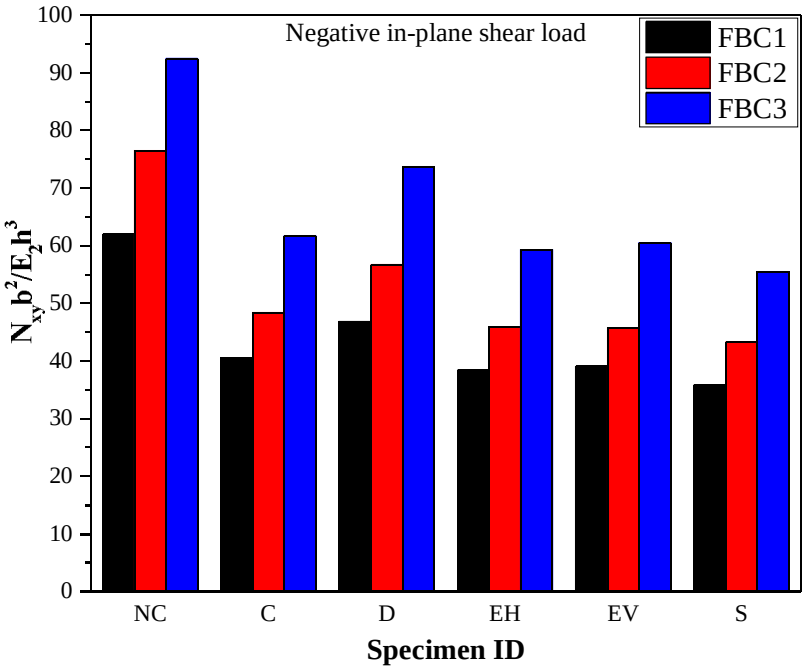

(b)

Fig. 5.21. First ply failure loads of functionally graded hybrid composite plates aligned in $(+45/-45/0/90)_{2s}$ direction with and without cutouts under: (a) Positive in-plane shear; (b) Negative in-plane shear

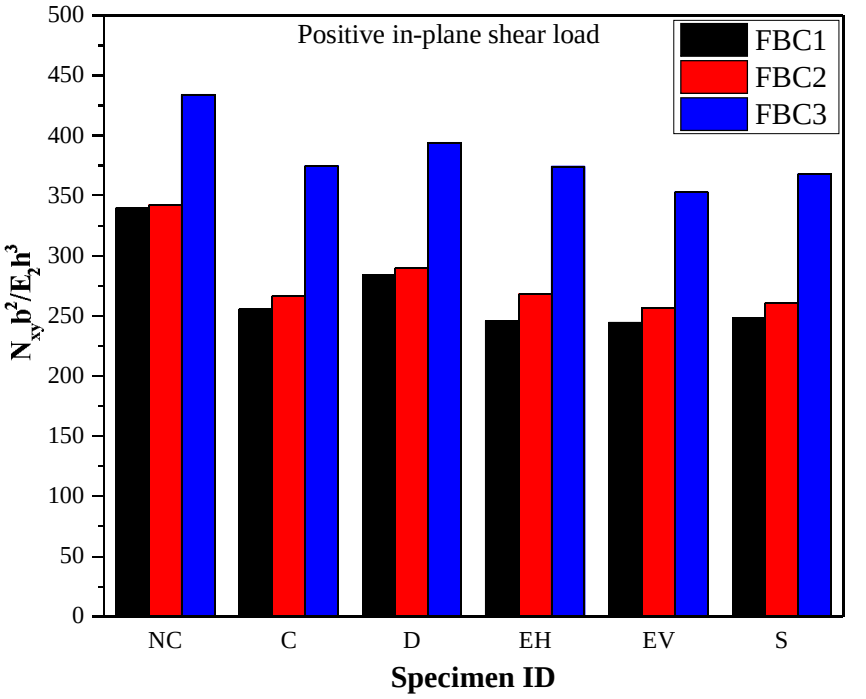

(a)

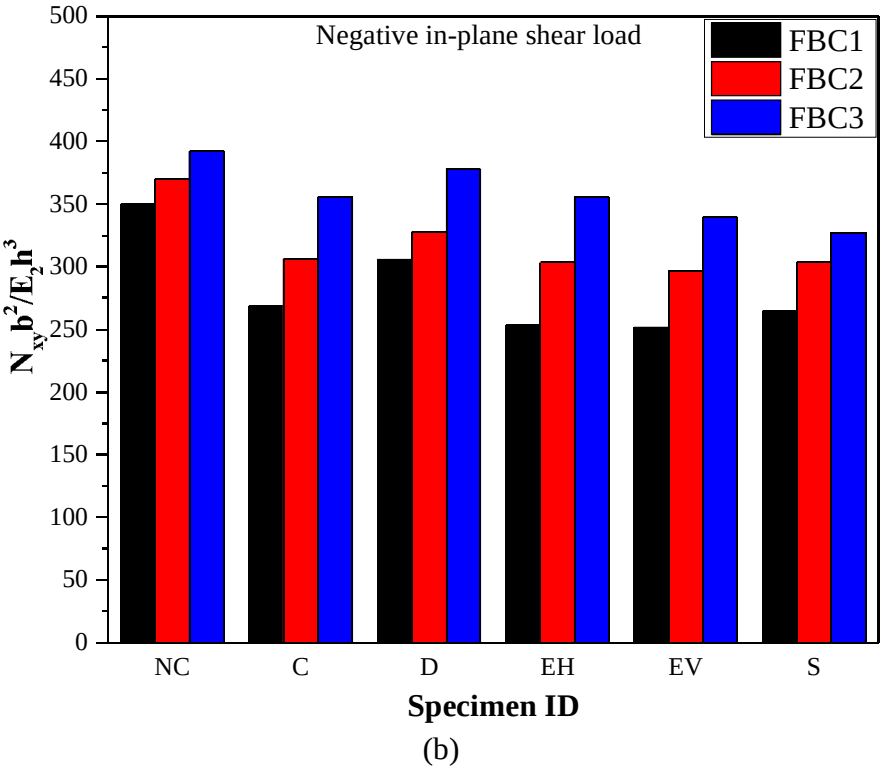

(b)

Fig. 5.22. Ultimate failure loads of functionally graded hybrid composite plates aligned in $(+45/-45/0/90)_{2s}$ direction with and without cutouts under: (a) Positive in-plane shear; (b) Negative in-plane shear

Similar trend is observed in first failure and ultimate failure loads as shown in Figs. 5.21(a), 5.21(b), 5.22(a), and 5.22(b). The minimum critical buckling and failure loads are observed in FH plates with FBC1 boundary condition having elliptical cutout aligned vertically as shown in Figs. 5.20(b) and 5.22(a); and also, the plates with square cutout as shown in Figs. 5.20(a), 5.21(a), 5.21(b), and 5.22(b). It is also observed that buckling and first failure loads are observed high in case of FH plates with FBC3 boundary condition subjected to negative in-plane shear load (Figs. 5.23(a) and 5.23(b)) while the ultimate failure load is observed high in case of FH plates with FBC3 boundary condition subjected to positive in-plane shear load as shown in Fig. 5.23(c).

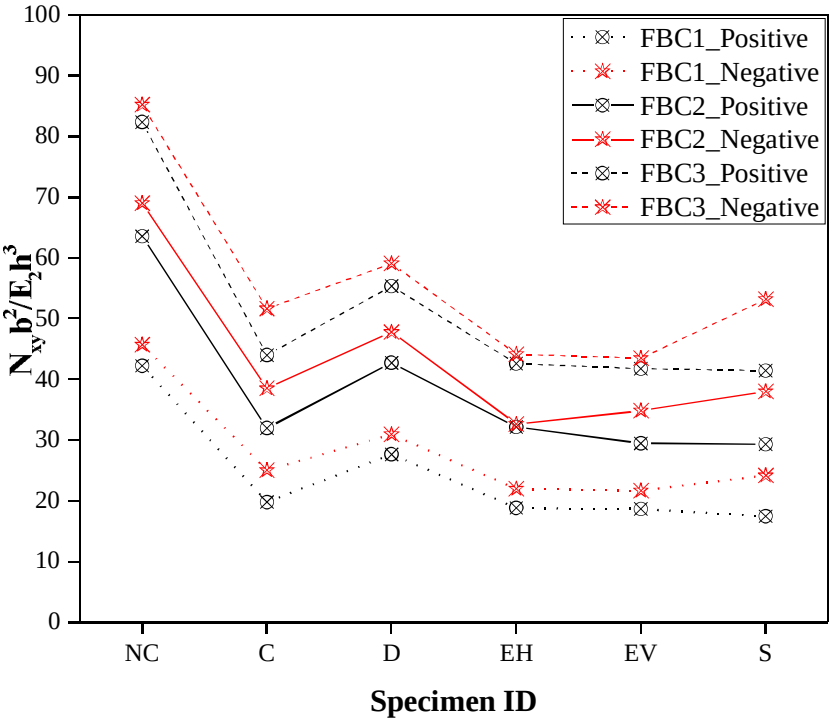

(a)

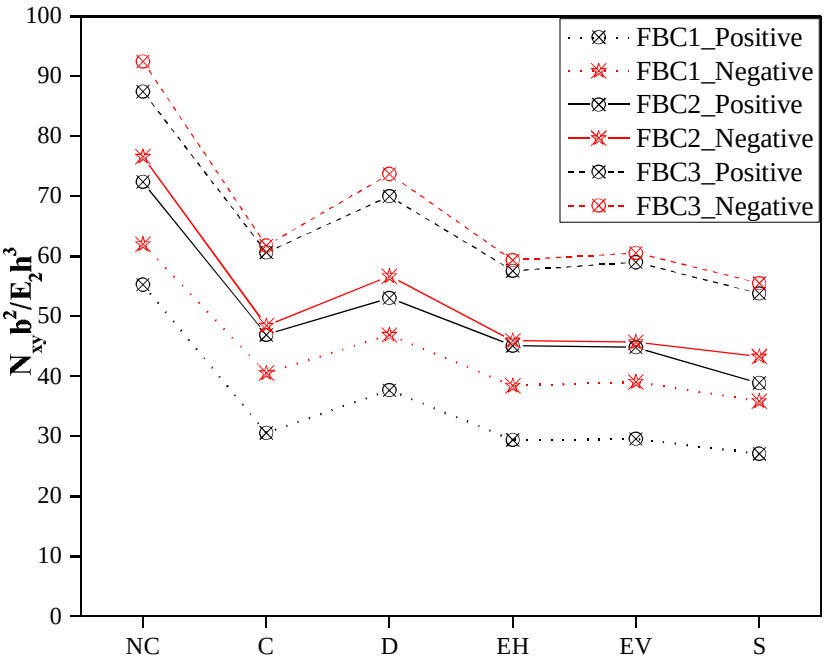

(b)

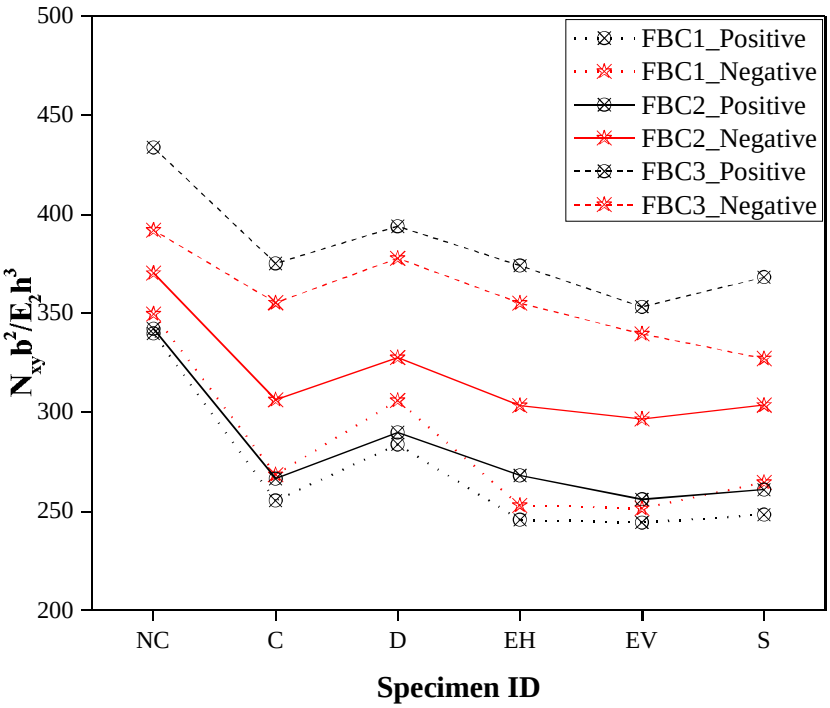

(c)

Fig. 5.23. Effect of direction of in-plane shear load of the plate aligned in $(+45/-45/0/90)_{2s}$ direction with different boundary conditions on: (a) Critical buckling loads; (b) First ply failure loads; (c) Ultimate failure loads

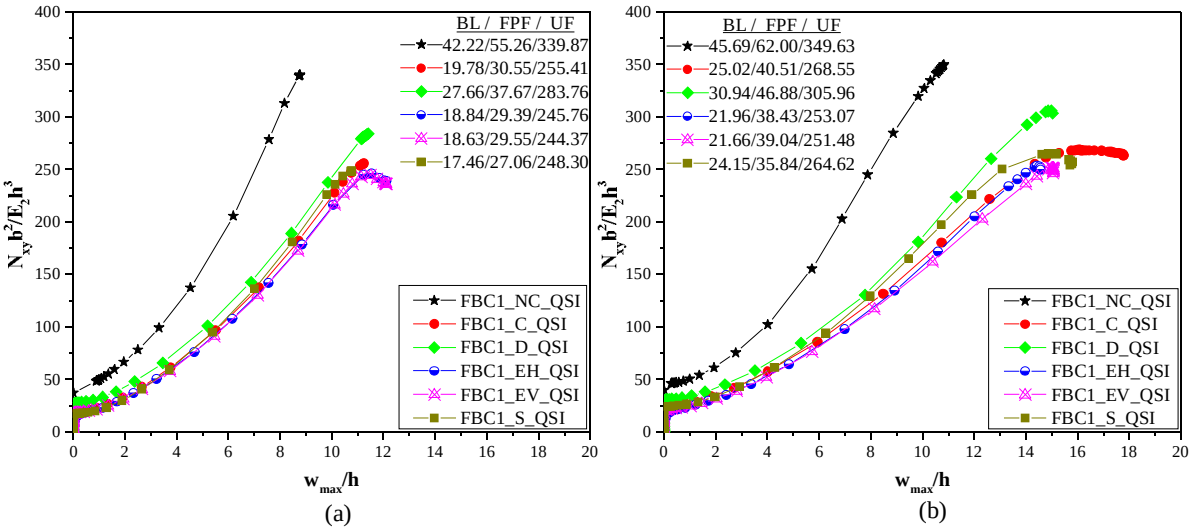

Fig. 5.24. Load deflection responses of functionally graded hybrid composite plates aligned in $(+45/-45/0/90)_{2s}$ direction with and without cutouts with all the edges simply supported (FBC1) under: (a) Positive in-plane shear load (b) Negative in-plane shear load

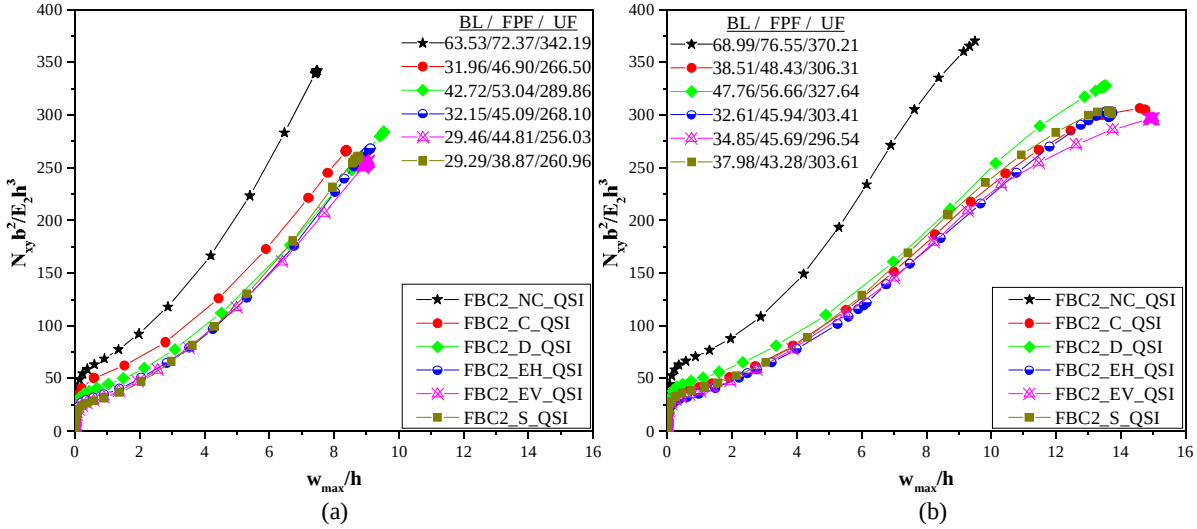

Fig. 5.25. Load deflection responses of functionally graded hybrid composite plates aligned in $(+45/-45/0/90)_{2s}$ direction with and without cutouts with two edges simply supported and other two edges clamped (FBC2) under: (a) Positive in-plane shear load (b) Negative in-plane shear load

From Fig. 5.24, it is evident that irrespective of cutout shape functionally graded hybrid composite plates aligned in $(+45/-45/0/90)_{2s}$ direction subjected to negative in-plane shear has highest buckling, first failure and ultimate failure loads. Also, FH plate without cutout has a different trend with respect to plates with cutouts irrespective of the applied shear loading direction. In case of

ultimate failure load, effect of boundary conditions (i.e., FBC1, FBC2, and FBC3) is not significant but the effect is significant for buckling and first ply failure loads.

The stiffness of plates under positive in-plane shear is higher compared to plates under negative in-plane shear load. Figure 5.25 shows that the load deflection response of FH plates with FBC2 boundary conditions (two opposite edges simply supported and the other two clamped). The buckling, first failure and the ultimate failure loads are higher in these plates when compared to the plates with all edges simply supported (Fig. 5.24). However, similar trend (Fig. 5.26) is observed in the plates with FBC3 boundary conditions. Figure 5.26 shows the load deflection response of FH plates with clamped boundary conditions on all the four ages (FBC3). In Fig. 5.26(b), it is observed that plates with elliptical cutouts aligned both horizontally and vertically follow similar trend. It is observed that FH plates subjected to positive in-plane shear load has highest ultimate failure loads comparatively.

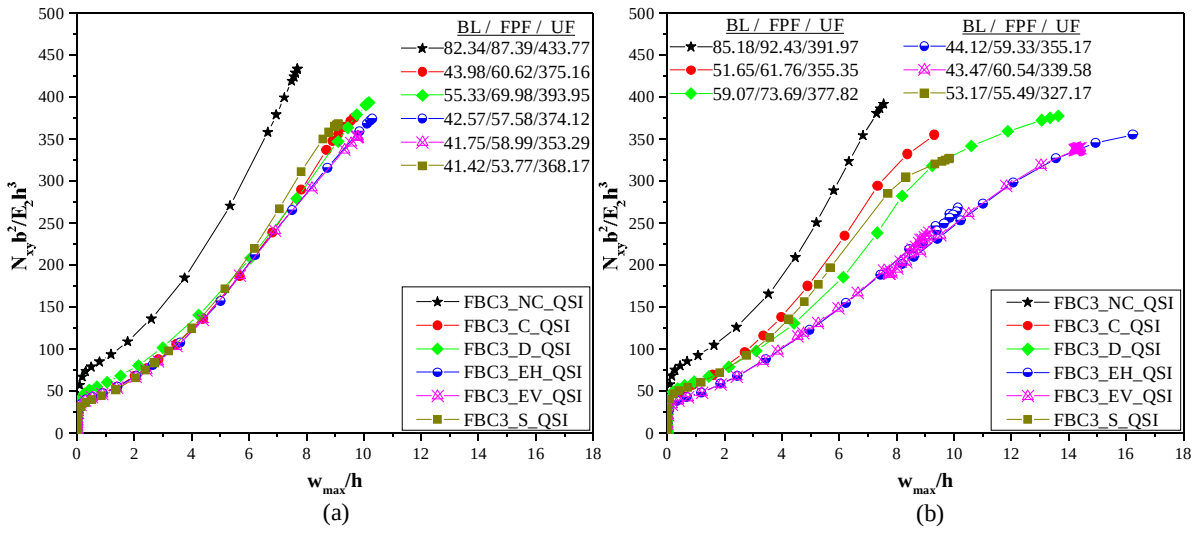

Fig. 5.26. Load deflection responses of functionally graded hybrid composite plates aligned in $(+45/-45/0/90)_{2s}$ direction with and without cutouts with all edges clamped (FBC3) under: (a) Positive in-plane shear load (b) Negative in-plane shear load

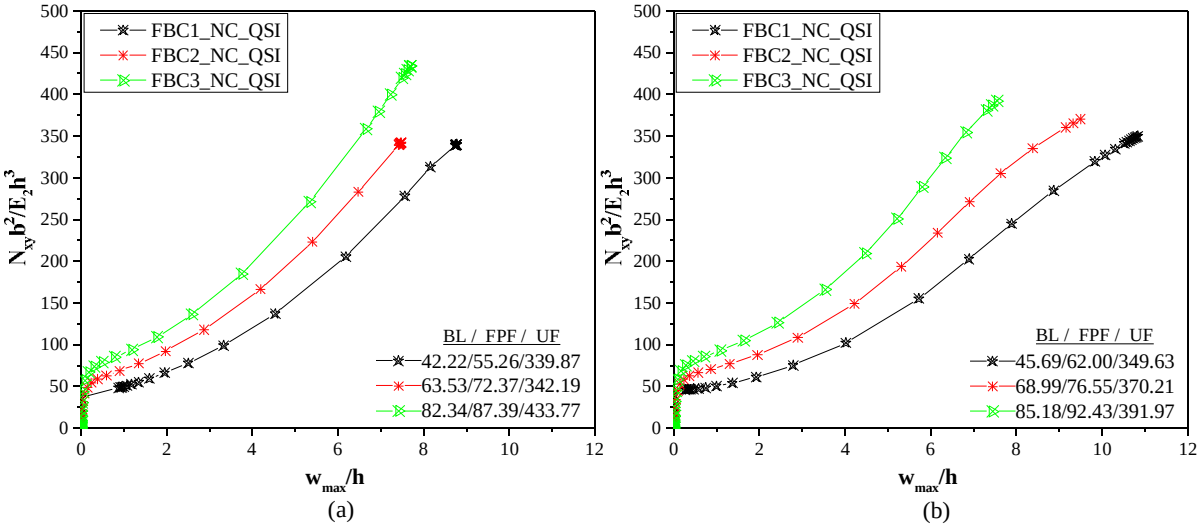

Fig. 5.27. Effect of flexural boundary conditions on postbuckling responses of functionally graded hybrid composite plates aligned in $(+45/-45/0/90)_{2s}$ direction without cutouts under: (a) Positive in-plane shear load (b) Negative in-plane shear load

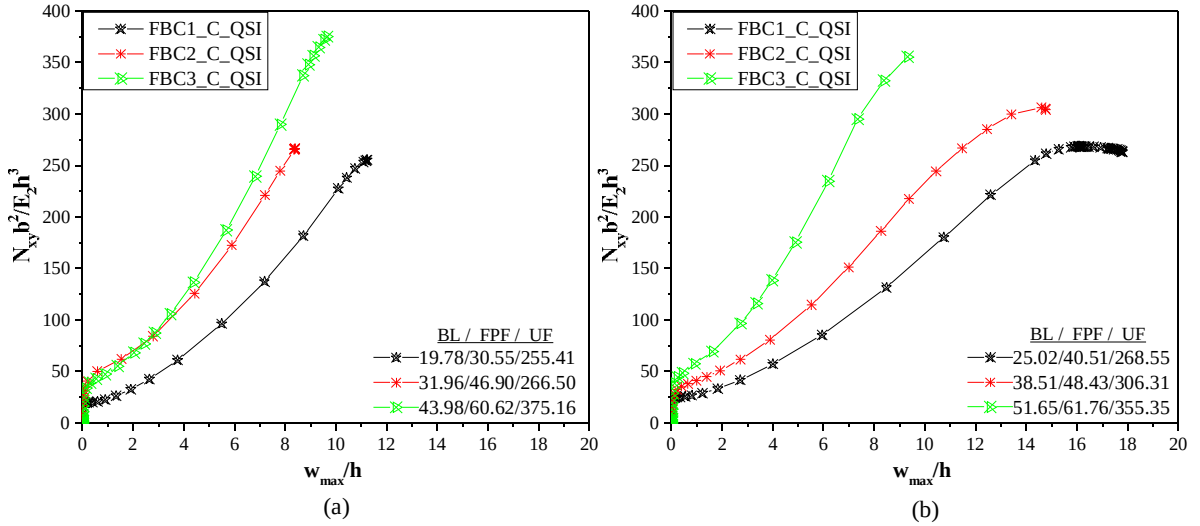

Fig. 5.28. Effect of flexural boundary conditions on postbuckling responses of functionally graded hybrid composite plates aligned in $(+45/-45/0/90)_{2s}$ direction with circular shaped cutouts under: (a) Positive in-plane shear load (b) Negative in-plane shear load

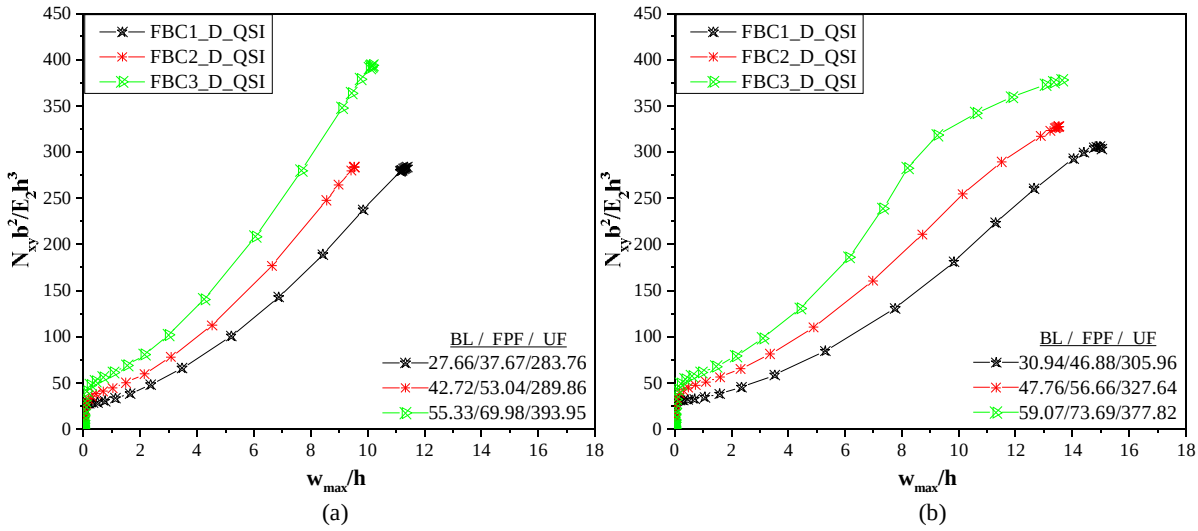

Fig. 5.29. Effect of flexural boundary conditions on postbuckling responses of functionally graded hybrid composite plates aligned in $(+45/-45/0/90)_{2s}$ direction with diamond shaped cutouts under: (a) Positive in-plane shear load (b) Negative in-plane shear load

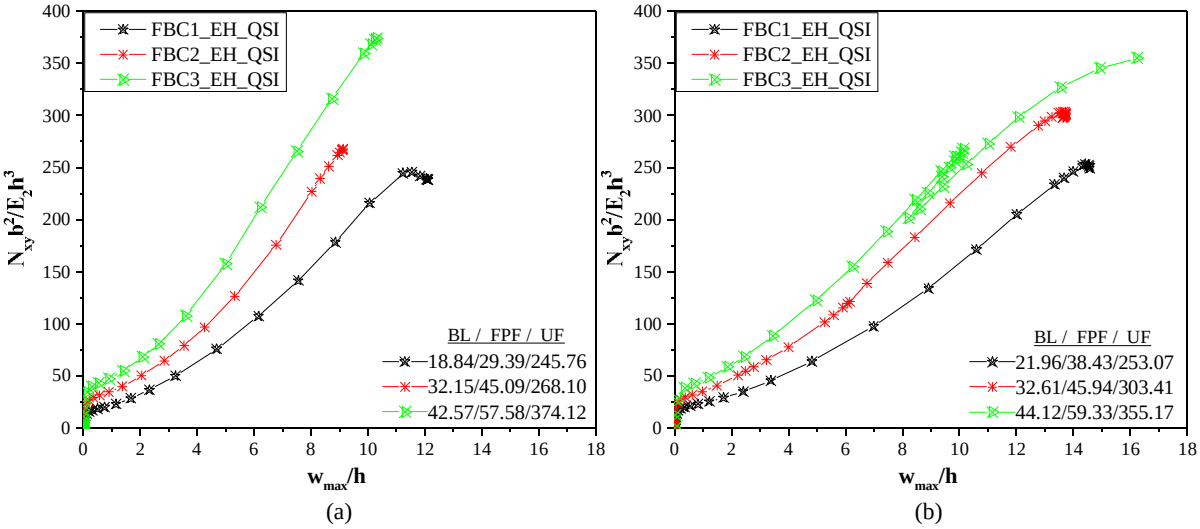

Fig. 5.30. Effect of flexural boundary conditions on postbuckling responses of functionally graded hybrid composite plates aligned in $(+45/-45/0/90)_{2s}$ direction with elliptical cutouts aligned horizontally under: (a) Positive in-plane shear load (b) Negative in-plane shear load

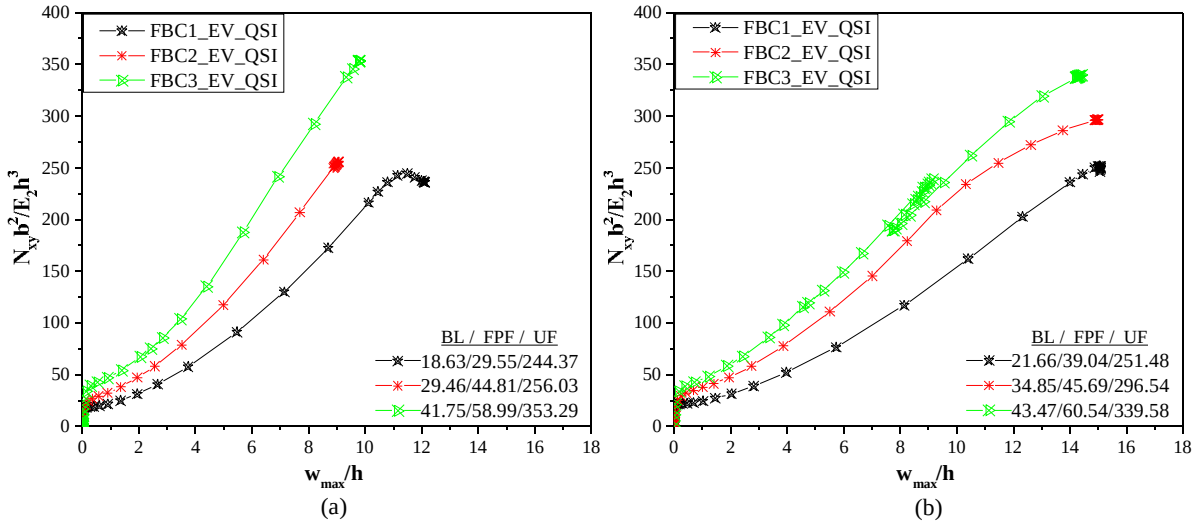

Fig. 5.31. Effect of flexural boundary conditions on postbuckling responses of functionally graded hybrid composite plates aligned in $(+45/-45/0/90)_{2s}$ direction with elliptical cutouts aligned vertically under: (a) Positive in-plane shear load (b) Negative in-plane shear load

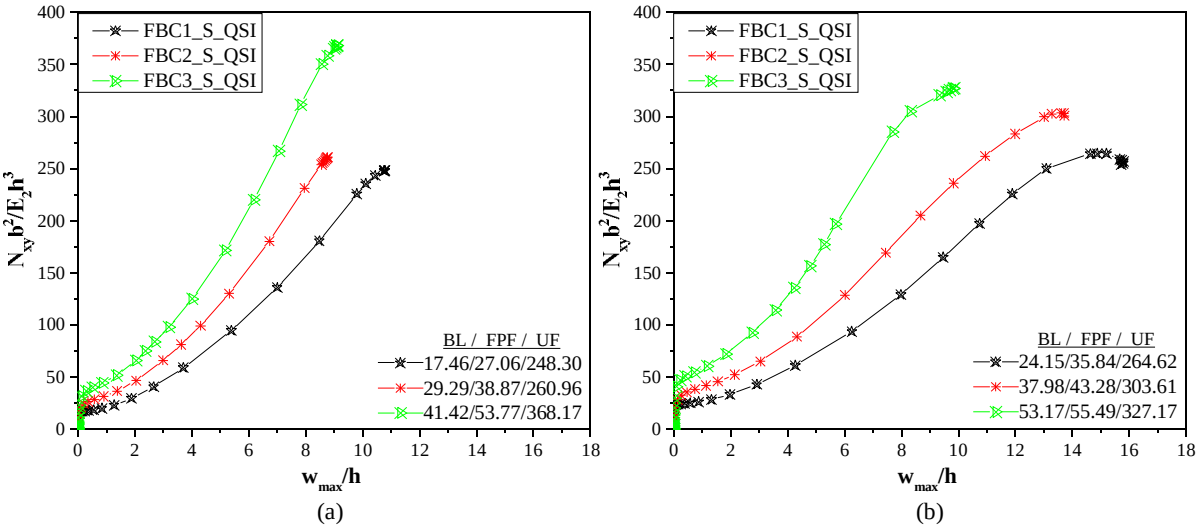

Fig. 5.32. Effect of flexural boundary conditions on postbuckling responses of functionally graded hybrid composite plates aligned in $(+45/-45/0/90)_{2s}$ direction with square shaped cutouts under: (a) Positive in-plane shear load (b) Negative in-plane shear load

Table 5.6. Buckling, first ply failure and ultimate failure loads of FH plates under positive and negative shear loads of stacking sequence $(+45/-45/0/90)_{2s}$ with different flexural boundary conditions

Specimen ID	FBC1		FBC2		FBC3	
	Positive In-plane Shear load	**Negative In-plane Shear load**	**Positive In-plane Shear load**	**Negative In-plane Shear load**	**Positive In-plane Shear load**	**Negative In-plane Shear load**
	BL♥/FPF♣/UL♠	BL♥/FPF♣/UL♠	BL♥/FPF♣/UL♠	BL♥/FPF♣/UL♠	BL♥/FPF♣/UL♠	BL♥/FPF♣/UL♠
FH_NC	42.2/55.3/339.9	45.7/62.0/349.6	63.5/72.4/342.2	69.0/76.5/370.2	82.3/87.4/433.8	85.2/92.4/392.0
FH_C	19.8/30.5/255.4	25.0/40.5/268.6	32.0/46.9/266.5	38.5/48.4/306.3	44.0/60.6/375.2	51.7/61.8/355.3
FH_D	27.7/37.7/283.8	30.9/46.9/306.0	42.7/53.0/283.9	47.8/56.7/327.6	55.3/70.0/393.9	59.1/73.7/377.8
FH_EH	18.8/29.4/245.8	22.0/38.4/253.1	32.2/45.1/268.1	32.6/45.9/303.4	42.6/57.6/374.1	44.1/59.3/355.2
FH_EV	18.6/29.6/244.4	21.7/39.0/251.5	29.5/44.8/256.0	34.8/45.7/296.5	41.7/59.0/353.3	43.5/60.5/339.6
FH_S	17.5/27.1/248.3	24.2/35.8/264.6	29.3/38.9/261.0	38.0/43.3/303.6	41.4/53.8/368.2	53.2/55.5/327.2

♥Buckling load; ♣First-ply failure; ♠Ultimate failure load

Note: All the values are non-dimensional (i.e., $N_{xy}b^2/E_2h^3$) where, N_{xy} is In-plane shear load; b is width of the plate; E_2 is transverse modulus; h is thickness of the plate

Table 5.7. Buckling, first ply failure and ultimate failure loads of FH plates under positive and negative shear loads of stacking sequence $(+45/-45/0/90)_{2s}$ with different in-plane boundary conditions

Specimen ID	PBC1		PBC2		PBC3	
	Positive In-plane Shear load	**Negative In-plane Shear load**	**Positive In-plane Shear load**	**Negative In-plane Shear load**	**Positive In-plane Shear load**	**Negative In-plane Shear load**
	BL♥/FPF♣/UL♠	BL♥/FPF♣/UL♠	BL♥/FPF♣/UL♠	BL♥/FPF♣/UL♠	BL♥/FPF♣/UL♠	BL♥/FPF♣/UL♠
FH_NC	109.0/96.9/571.1	115.4/91.0/582.5	39.7/65.5/336.6	42.5/62.9/337.4	31.4/40.0/420.5	33.6/38.9/434.6
FH_D	93.1/95.6/582.1	98.5/92.1/548.3	21.4/32.3/295.2	22.9/33.5/311.7	18.9/25.6/369.9	20.2/25.9/364.2

♥Buckling load; ♣First-ply failure; ♠Ultimate failure load

Note: All the values are non-dimensional (i.e., $N_{xy}b^2/E_2h^3$) where, N_{xy} is In-plane shear load; b is width of the plate; E_2 is transverse modulus; h is thickness of the plate

Among all the FH plates with cutouts, diamond shaped cutout plate has the highest buckling load irrespective of the types of boundary condition and the directions of shear loads applied. Further, comparison of load vs. deflection of FH plates without cutout with different flexural boundary conditions is presented in Fig. 5.27. Plates without cutout, with circular, diamond, ellipse aligned horizontally and vertically, and square shaped cutouts are presented in Figs. 5.27, 5.28, 5.29, 5.30, 5.31 and 5.32, respectively. In this comparison, plates with all four edges clamped show maximum postbuckling strength and plates with all edges simply supported show lower postbuckling strength, irrespective of direction of applied in-plane shear loads. Although, plates without cutouts have maximum postbuckling strength, diamond shaped cutout FH plate has better performance among plates with cutouts. The corresponding load values of these plates are depicted in Table 5.6.

Further, plates with diamond shaped cutouts and plates without cutouts are checked with simply supported boundary condition having in-plane boundary conditions (PBC1, PBC2, and PBC3) as shown in Fig. 5.33. In this, response of plates is predicted by simulating the in-plane boundary restraints as shown in Fig. 5.20. FH plates without cutout under positive and negative in-plane shear loads are shown in Figs. 5.33(a) and 5.33(b), respectively while plates with diamond shaped cutout are presented in Figs. 5.33(c) and 5.33(d), respectively.

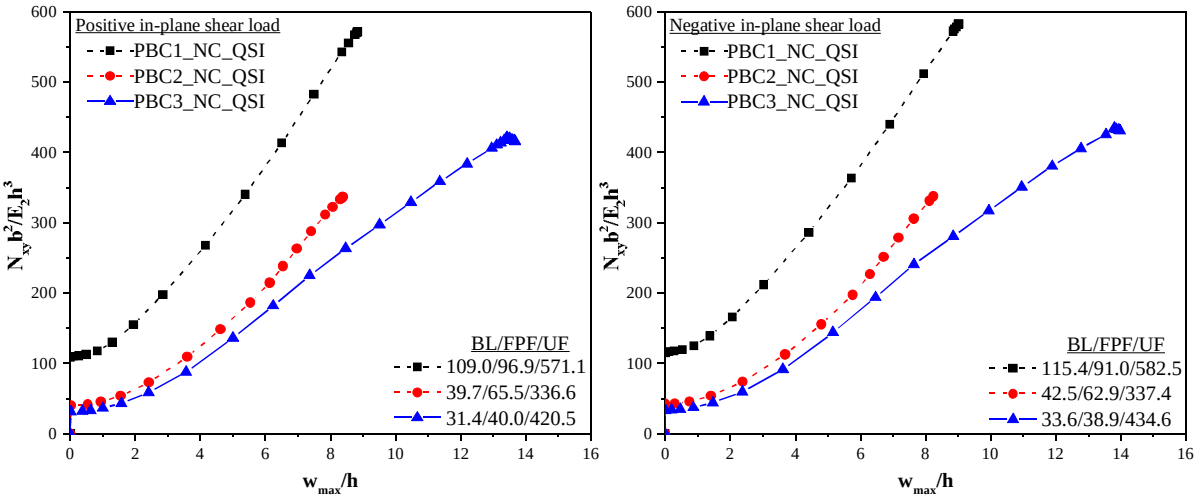

(a) (b)

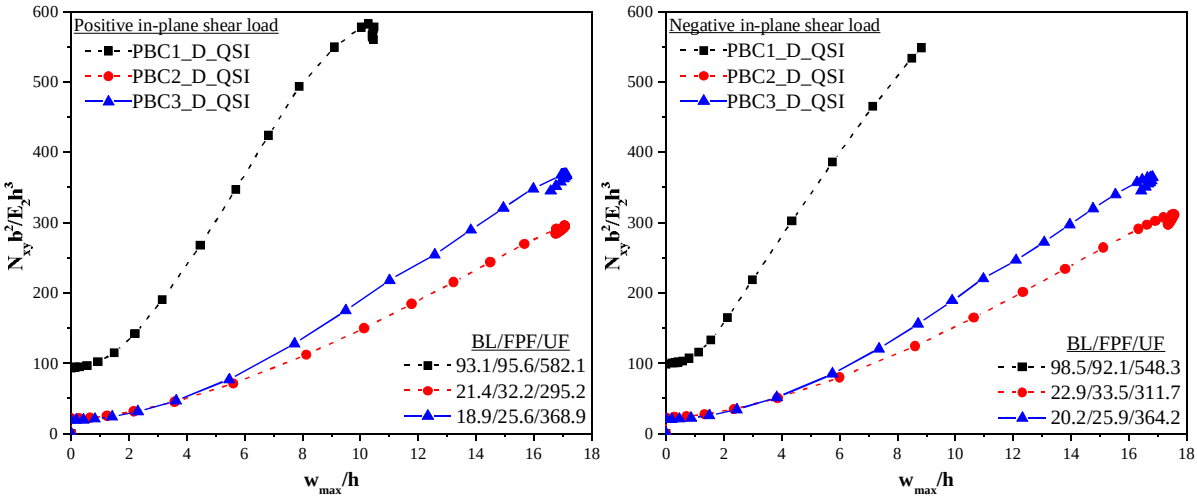

(c) (d)

Fig. 5.33. Effect of in-plane boundary conditions on postbuckling responses of simply supported functionally graded hybrid composite plates aligned in $(+45/-45/0/90)_{2s}$ direction (a) without cutout under positive in-plane shear load and (b) without cutout under negative in-plane shear load (c) with diamond shaped cutout under positive in-plane shear load and (d) with diamond shaped cutout under negative in-plane shear load

In all the cases, the buckling and postbuckling strength is observed to be highest in FH plates with PBC1 boundary conditions irrespective of presence of cutout and applied shear load directions. In case of plates with PBC2 and PBC3 boundary conditions, the critical buckling and first ply failure loads are higher in plates with PBC2 boundary conditions irrespective of presence of cutout and applied shear load directions. Though PBC2 plates has maximum buckling and first ply failure loads, the ultimate failure loads are observed to be higher in PBC3 plates. Therefore, postbuckling strength has a significant effect in functionally graded hybrid plates with in-plane boundary restraint PBC3. The corresponding load values of plates with in-plane boundary conditions are depicted in Table 5.7. Critical buckling loads are higher in plates subjected to negative in-plane shear loads is one of the major observations, irrespective of type of boundary conditions i.e., either flexural or in-plane boundary conditions.

5.5. Concluding remarks

Based on the study of numerical investigation of postbuckling response of functionally graded hybrid composite plates with and without cutouts subjected to inplane shear loading, the following concluding remarks can be made:

1. The maximum critical buckling and first ply failure loads are observed in functionally graded hybrid (FH) composite plates subjected to negative in-plane shear load than FH plates subjected to positive in-plane shear load. The response is poor in plates under positive in-plane shear.
2. The FH plates with fiber aligned in (+45/-45) direction are observed to have highest critical buckling loads in comparison to the plates with fibers aligned in (0/90) and (+45/-45/0/90) directions.
3. The FH plates having stacking sequence of $(+45/-45)_{4s}$ has the highest maximum first ply failure loads when the plates are subjected to negative in-plane shear load.
4. In case of FH plates subjected to negative in-plane shear load, the FPF loads are higher in fibers aligned in (+45/-45/0/90) direction except the plate without cutout. The highest FPF load of plate without cutout is observed in plate with fiber aligned in (+45/-45) direction.
5. Amongst the plates with different shaped cutouts, FH plates with diamond shaped cutouts perform better irrespective of directions of in-plane shear loads and fiber directions.
6. FH plates with small sized cutouts perform better in terms of critical buckling and first ply failure loads. Also, the FH plate with small sized cutout outperforms irrespective of fiber direction, shape of cutout, and direction of applied in-plane shear loads.
7. The functionally graded hybrid composite plates without cutouts has higher buckling and first failure loads with FBC3 flexural boundary condition.
8. Among the FH plates with different shaped cutouts, diamond shaped cutout plate with FBC3 boundary condition show better performance irrespective of the directions of applied shear loads. Hence, there is an effect of cutout shape on the buckling and postbuckling responses of composite plates.
9. Amongst all the flexural boundary conditions considered in this study, FH plates with all four edges clamped (FBC3) has better buckling and failure loads irrespective of the directions of shear load. It has been concluded that boundary conditions have a major effect on the buckling and postbuckling strengths of composite plates irrespective of the cutout shapes and directions of applied shear loads.
10. In plates with FBC1 and FBC2 boundary conditions, initial buckling and failure loads are higher for negative in-plane shear loaded plates. In case of FH plates with FBC3 boundary condition, ultimate failure loads are higher in positive in-plane shear loaded plates.

Therefore, effect of direction of in-plane shear is significant in plates with FBC3 boundary conditions.

11. In case of functionally graded hybrid composite plates without cutouts and with in-plane boundary conditions, PBC1 has better buckling and postbuckling strengths irrespective of the presence of cutout and applied shear load directions.
12. Amongst the plates with PBC2 and PBC3 boundary conditions, the plate with PBC2 boundary condition is having maximum buckling and first failure loads. However, the postbuckling strength is higher in plates with PBC3 boundary condition since it has peak ultimate failure load compared to plates with PBC2 boundary condition.